Fall 2013

Study of artificially disordered optical fibers

Herath Mudiyanselage Sumudu Rasika Kumari Herath

Department: Physics

STUDY OF ARTIFICIALLY DISORDERED OPTICAL FIBERS

by

HERATH MUDIYANSELAGE SUMUDU RASIKA KUMARI HERATH

A DISSERTATION

Presented to the Faculty of the Graduate School of the

MISSOURI UNIVERSITY OF SCIENCE AND TECHNOLOGY

In Partial Fulfillment of the Requirements for the Degree

DOCTOR OF PHILOSOPHY

in

PHYSICS

2013

Approved by

Dr. Alexey Yamilov, Advisor
Dr. Jerry Peacher
Dr. Rosa Zheng
Dr. John Story
Dr. Jie Gao

DEDICATION

This dissertation is dedicated to my parents and all the teachers who provided the knowledge, guidance and moral support to accomplish my goals.

PUBLICATION DISSERTATION OPTION

This dissertation has been prepared in the form of three papers. Paper I, pages 12–37 had been published as *Fabrication, characterization and theoretical analysis of controlled disorder in the core of the optical fibers*, Applied optics **50**, 802 (2011) with N.P.Puente, E.I.Chaikina, and A.Yamilov. Paper II, pages 38–61 had been published as *Artificially disordered birefringent optical fibers*, Optical express **20**, 3620-3632 (2012) with N.P.Puente, E.I.Chaikina and A.Yamilov. Paper III, pages 62–71 had been published as *Investigation of mode coupling in optical fiber with controlled volume disorder*, SPIE Proceedings: Specialty Optical Fibers and Their Applications **7839**, 78391O-1(2010) with N.P.Puente, E.I.Chaikina, and A.Yamilov.

ABSTRACT

Light transmission through photo-sensitive multi-mode fibers (MMF) with controlled volume disorder is investigated. Experiment shows that a segment of disordered MMF as short as 10 cm is sufficient to distribute power uniformly over all co-propagating modes and the intensity at the output surface of the fiber follows the Rayleigh negative exponential function. To explain the experimental findings, a comprehensive theoretical model is developed with three main results.

First, statistical properties of all components of the dielectric tensor are obtained and analyzed in the framework a microscopical model of photo-sensitivity in a germano-silicate glasses. Secondly, it is shown that induced birefringence is insufficient to explain mode mixing, and that cross-polarization mode coupling is essential. Such a coupling is shown to originate from the spatial correlation in the off-diagonal elements of the dielectric tensor. Third, a hybrid theory to describe propagation in a fiber with a spatially correlated disorder is developed. The proposed theory treats the deterministic part of the light via coupled-amplitude equations, and the randomly-phased component with coupled-power equations.

The complete theory developed in this work has a predictive power – it can guide the design of an artificial disorder based on the desired transmission properties of the fiber. Experiment shows that mixing all co-propagating modes can, indeed, be attained in a short segment of a suitably designed disordered MMF without a prohibitive loss. Such fibers can be useful for e.g. maximizing the information capacity multi-mode fiber links.

ACKNOWLEDGMENTS

Many individuals contributed either directly or indirectly to not only the success of this particular project but also my graduate experience as a whole at Missouri University of Science and Technology.

First and foremost, I want to express my appreciation to my research advisor, Dr. Alexey Yamilov, for his motivating influence and constant support. It was through his encouragement that I was brought into this very interesting field. His work habits, organization and analytical approach to problem solving will guide me throughout remainder of my career. I am also grateful to Dr. Jerry Peacher, my academic advisor, and Dr. George Waddill, Physics Department chairman for their kind and invaluable support in so many situations during the years of my graduate studies. Sincere appreciation is expressed to the members of my doctoral committee: Dr. Alexey Yamilov, Dr. John Story, Dr. Jerry Peacher, Dr. Rosa Zheng, and Dr. Jie Gao. Their assistance and guidance aided me in accomplishing my goal.

I would like to offer special thank you all of friends, my colleagues, and the Physics Department staff members at Missouri S& T.

I extend, my deepest gratitude to my family. My father, Sunil Herath, served as a constant source of inspiration. I would not have been able to realize these achievements without unwavering love and support I received from my mother, Nandanee Ranaweera. My brother, Dr. Dumindu Herath encouraged me with love and moral support, and my husband, Dr. Nilanka Gurusinghe, kept my hope alive while on this journey. I am also grateful to my dear son, Savain Gurusinghe. His smiles, laughter, hugs, and kisses always helped ease the tension and put things in perspective.

This work was supported by the University of Missouri Research Board and the National Science Foundation Grant No. DMR-0704981.

TABLE OF CONTENTS

Page

LIST OF ILLUSTRATIONS

Figure Page

1. INTRODUCTION

1.1. OPTICAL FIBERS IN COMMUNICATION

1.1.1. Historical Perspective. Presently, both long and medium range data communication are dominated by optical fibers. Using light in communication has increased the information transfer rate by a factor of 10 every four years. New methods and devices had to be developed to sustain such an enhancement. These advances were largely enabled by two basic ideas dating back to the nineteenth century. The first idea was formulated in the mid-19th century by Daniel Colladon and John Tyndall [1], see Fig.1.1, which described a "light pipe" that can guide light along a curved path due to the effect of total internal reflection. The second idea came from Alexander Graham Bell who, in 1880, invented a "photo-phone" [2], as shown in Fig.1.2. In this device, the light beam intensity was modulated by an audio signal in a flexible mirror; and modulated light beam was then transmitted through the air. The receiver demodulated the signal by a photo-sensitive material that changed its resistivity in response to variations of light intensity. The photo-phone was ultimately found to be impractical due to instabilities in the atmosphere that created fluctuations, degrading the signal's quality. This early setback highlighted the importance of maintaining an orderly flow of light from the transmitter to the receiver.

Combining the ideas behind the light-pipe and the photo-phone led to the development of early optical fibers. It initially appeared that the problems plaguing the photo-phone could be eliminated by replacing the over-the-air transmission channel with fluctuation-free glass fiber. The first study to examine the possibility of using optical fibers commercially for data transmission [5] concluded that the distance over

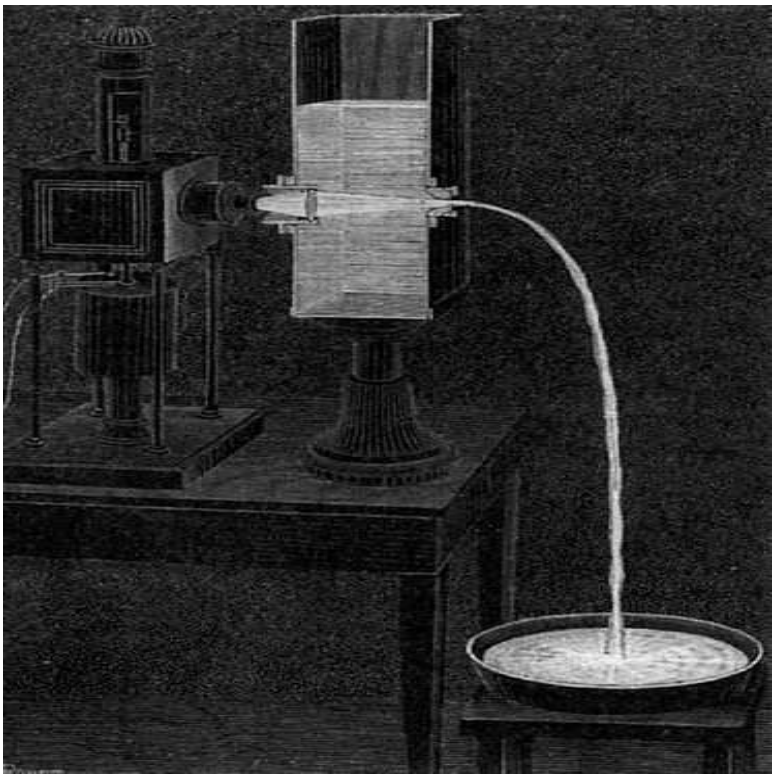

Figure 1.1: Light propagation in a curved path due to total internel reflection [3]. This effect was initially demonstrated by Daniel Colladon and further popularized by John Tyndall.

which the communication could be achieved was limited largely by Rayleigh scattering on imperfections in the medium. Once again, optical communication was set back by a disorder (albeit of a different kind) in the transmission channel. The development of ultra-pure glasses by Corning Glass, together with erbium-doped fiber amplifiers, led to revolution in the development optical communication [6].

1.1.2. Information Capacity of Optical Fiber. During the initial research and development of optical fibers, the single-mode fiber (SMF) emerged as a de-facto standard for long-range communication [7]. The proliferation of audio- and video-communication and the internet led to an ever-increasing demand for network capacity. It also stimulated research to increase the transmission capacity of

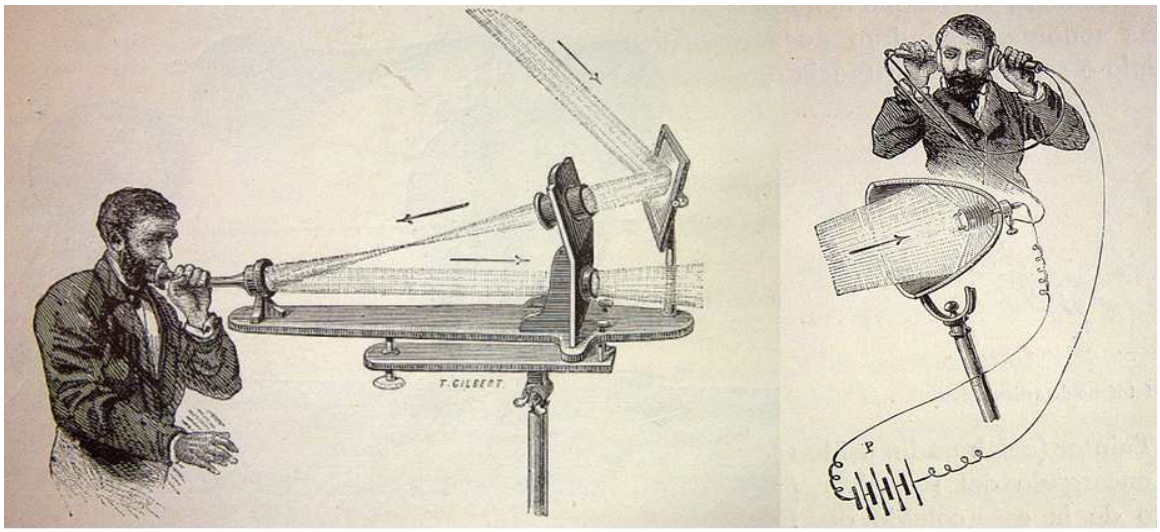

Figure 1.2: Alexander Graham Bell invented the photo-phone in 1880 [4]. This was the first demonstration of the basic principle of the long-range optical communication.

SMF [8]. Thus far, the demand has been met – various techniques, including both dense wavelength division multiplexing and advanced high efficiency coding, led to a ten-fold increase in demonstrated capacity every four years over the last thirty years. However, current projections suggest that the available network capacity will be exhausted around the year 2015 [8].

Studies of the fundamental limits have shown [9, 10, 11] that the information capacity of an optical channel is given by

$$C = \mathrm{WDM} \times \log_2 \left[\det \left(\hat{I} + \mathrm{SNR} \times (1/N) \hat{t} \hat{t}^{\dagger} \right) \right] \text{ bits s}^{-1} \text{ Hz}^{-1}, \tag{1.1}$$

where WDM is the wavelength division multiplexing factor, SNR is a signal-to-noise ratio, $\hat{I}$ is an $N \times N$ unitary matrix, and $\hat{t}$ is an $N \times N$ matrix which describes

transmission through the channel. Currently, increasing WDM and SNR factors has been exhausted in dense wavelength division multiplexing and high efficiency coding approaches, respectively. The former is limited by the gain bandwidth in the erbium-doped fiber amplifiers [12], and the latter is constrained by non-linear effects that distort the high-intensity signal [13, 14, 15].

1.1.3. Space Division Multiplexing. Equation (1.1) reveals that information capacity can be further increased if the number of fiber's spatial degrees (modes in e.g., a multi-mode (MMF) or a multi-core fiber (MCF) [16], see Fig.1.3) is increased. In essence, increasing N allows one to increase SNR without producing the detrimental effects of non-linearities because the power is distributed over many modes. Although the idea of using MMF and MCF dates back to the early days of fiber communication [17, 18], it has only recently become the focus of intense research. This research has been stimulated by the convergence of technological advances and practical need [16].

The difficulty that impedes wide-spread use of MMF in communication is a result of the added complexity in independently addressing and detecting individual fiber modes. Furthermore, mode-mixing during propagation limits the maximum length of the fiber, for which such approach can be still utilized. Another drawback of MMF is modal dispersion [19] – light propagates at different velocities in different modes.

It has been pointed out [11] that, to achieve an increased capacity in Eq. (1.1), the matrix $\hat{t}$ does not need to be diagonal, as it is in the case of completely non-interacting modes. If the matrix is both known (e.g., via a series of training pulses) and invertable, the communication can proceed with an increased information capacity. The theoretical limit on improving a transmission signal's bandwidth is proportional to the number of sources/receivers. Such an approach has become known as the multiple-input-multiple-output (MIMO) technique [20] and is widely used in the

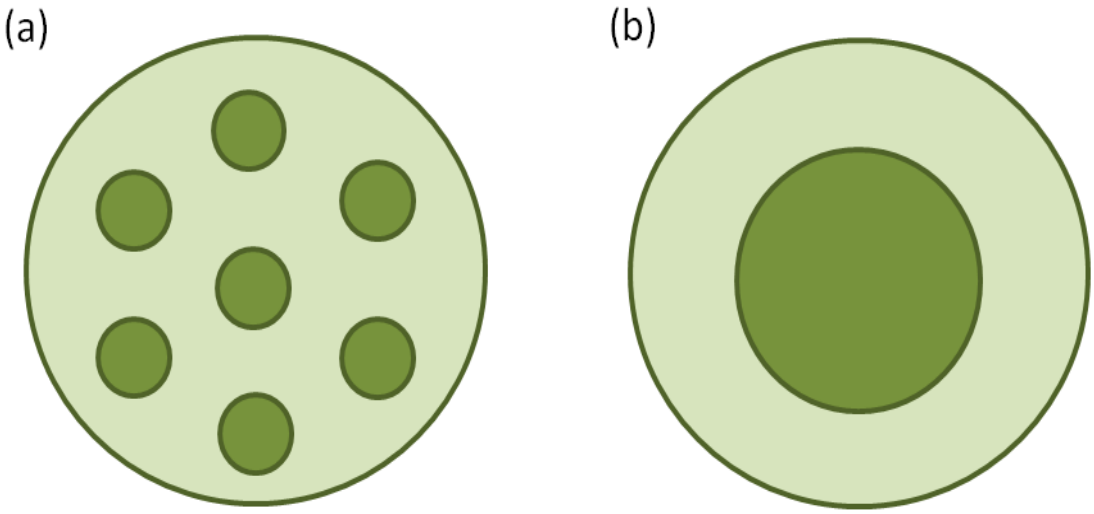

Figure 1.3: Cross sections of (a) multi-core and (b) multi-mode fibers.

wireless communication; it has become the backbone of IEEE 802.11n standard (and its successors) for local area networks (LANs) [9, 10, 21]. The same MIMO technology can also be applied to unlock the information capacity of multi-mode-fibers [20, 22].

1.1.4. Mode Coupling. Researchers have formulated numerous approaches, such as M-ary coding [23], electronic equalization [24, 25], and sub-carrier multiplexing, selective modal excitation [26], to maximize the capacity of MMF. Largely because these approaches are complex and costly, their practical implementation has been limited. Theoretical analysis of a multi-channel system's information capacity, has shown that it is maximized if the elements of the transmission matrix $\hat{t}$ are random-Gaussian [10]. This limit can be achieved if one radically changes the view on modal coupling – rather than minimizing it, one has to promote mode coupling [27].

Mode coupling causes the exchange of power among modes during signal propagation. In a MMF, mode coupling leads to a statistical equilibrium (i.e., equilibrium mode distribution) after certain characteristic length has been traversed [28, 29]. One can intentionally increase mode coupling in a MMF by introducing either bends [30, 31], stresses, or random imperfections. Obtaining fully coupled modes in conventional fibers requires sufficiently long segments of MMF, this is because concentration of imperfections is low. In the most disordered case of plastic optical fibers, the characteristic length for mode mixing is on the order of $10m$ [32].

The primary goal of this study is to introduce a different technique to excite all modes equally in a short segment of fiber (10cm) and therefore, to enhance the communication capacity. To achieve this goal, an artificial disorder is introduced in a photo-sensitive multi-mode step-index Germanium-doped silica fiber [33], see Fig.1.4. Doping by germanium atoms leads to an oxygen-deficient defect formation [34]. Illumination by a UV source with a sufficiently short wavelength breaks these bonds that, in turn, modifies the absorption spectrum of the glass. The real part of the refractive index is changed through the Kramers-Kronig relation. Such approach been used before to laser-write a wide variety of fiber gratings [35].

In this work, we developed a method for fabricating a controllable artificial disorder in the photo-sensitive fiber. We demonstrate that unlike the disorder which occurs in fibers naturally, the artificial disorder can be manipulated to promote mode coupling while at the same time suppressing the radiative loss.

1.1.5. Radiative Loss. Radiative loss is the attenuation of the light beam's intensity as it travels through the fiber's core. It is caused by e.g. scattering from the rough fiber wall, the finite size of the cladding, or inhomogeneities in the fiber's material [29], see Fig.1.5. Managing these losses in an optical fiber is important when a light signal is transmitting through the long fiber. The radiative loss due to

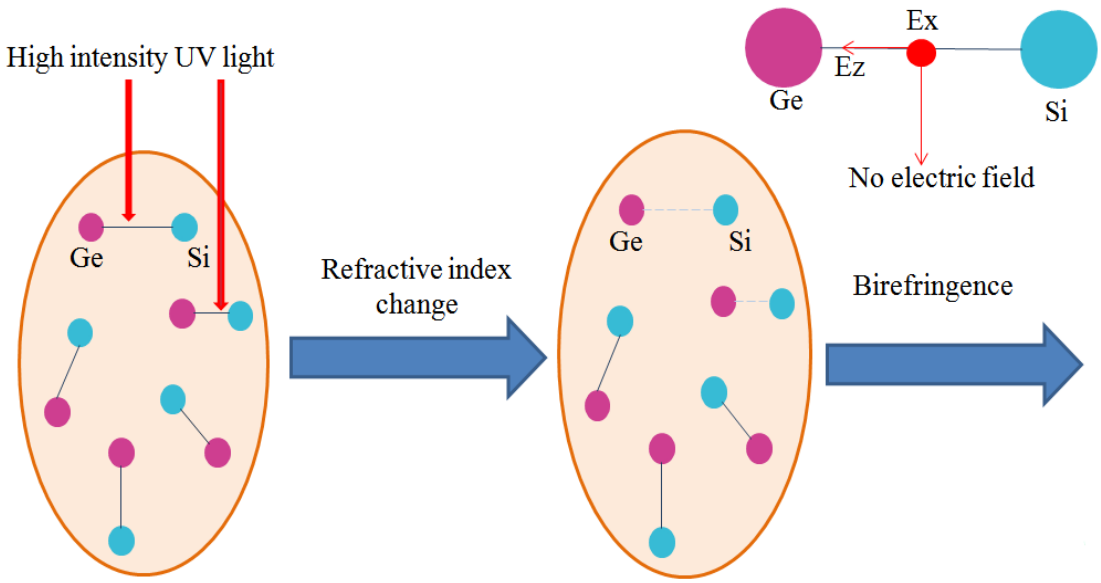

Figure 1.4: Doping of silica fiber with Ge creates highly directional Ge-Si bonds which can be broken by illuminating with UV light. This causes the refractive index to change.

Rayleigh scattering on molecular inclusions introduced in its fabrication process is the dominant loss mechanism in a glass fiber.

In conventional fibers, the Rayleigh scattering is responsible for both mode coupling and radiative loss [36]. Therefore, increase in mode coupling is inevitably accompanied by increased losses. In contrast, this study, demonstrates that in optical fibers with purposefully introduced modulations of the refractive index, one can promote mode coupling while maintaining a manageable amount of loss.

1.2. EXPERIMENTAL WORK

The experimental setup in this study is designed to inscribe volume disorder in the Ge-doped fiber core by exposing it to UV light from frequency-doubled Argon-ion laser with an operating wavelength of 244nm. Doping by Ge created weak, highly

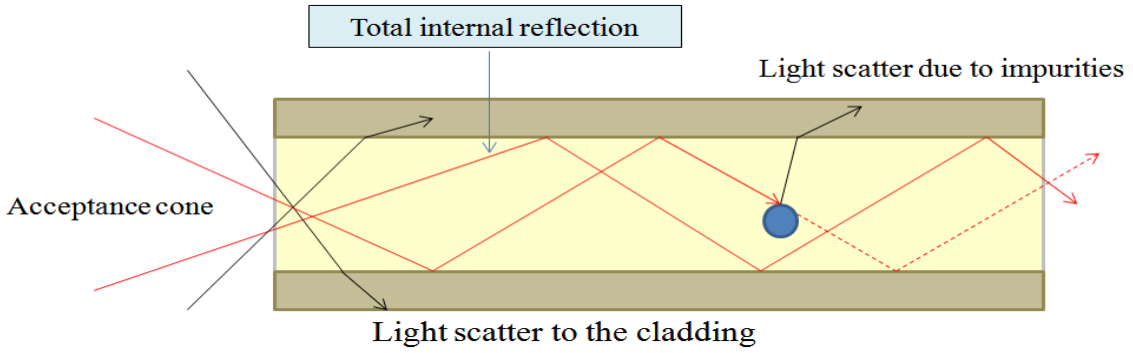

Figure 1.5: Light propagates in the core of the fiber due to total internal reflection and scatters to the cladding due to impurities. The latter called radiative loss.

directional Ge-Si bonds that could be broken by the short wavelength UV light. The unpolarized UV light passed through a diffuser creating a speckle fluctuation pattern with both high and low intensities [37]. In the region of high intensity, the refractive index is modified [33] and, thus, a disorder in the core is introduced.

Once the disorder has been created, 543nm light is used to perform transmission measurements, see Fig. 1.7. The fiber is illuminated with a linearly polarized light. The output light is detected separately by in both orthogonal polarization channels. The results of experimental measurement are explained using new theory developed in this work.

1.3. THEORETICAL WORK

The artificial disorder introduced in the experimental setup in Fig. 1.6 differs markedly from the Rayleigh-type commonly encountered in optical fibers. Scatterer can no longer be approximated as point. Furthermore, special attention has to be paid to the photo-induced birefringence, introduced by the polarized light [38] used

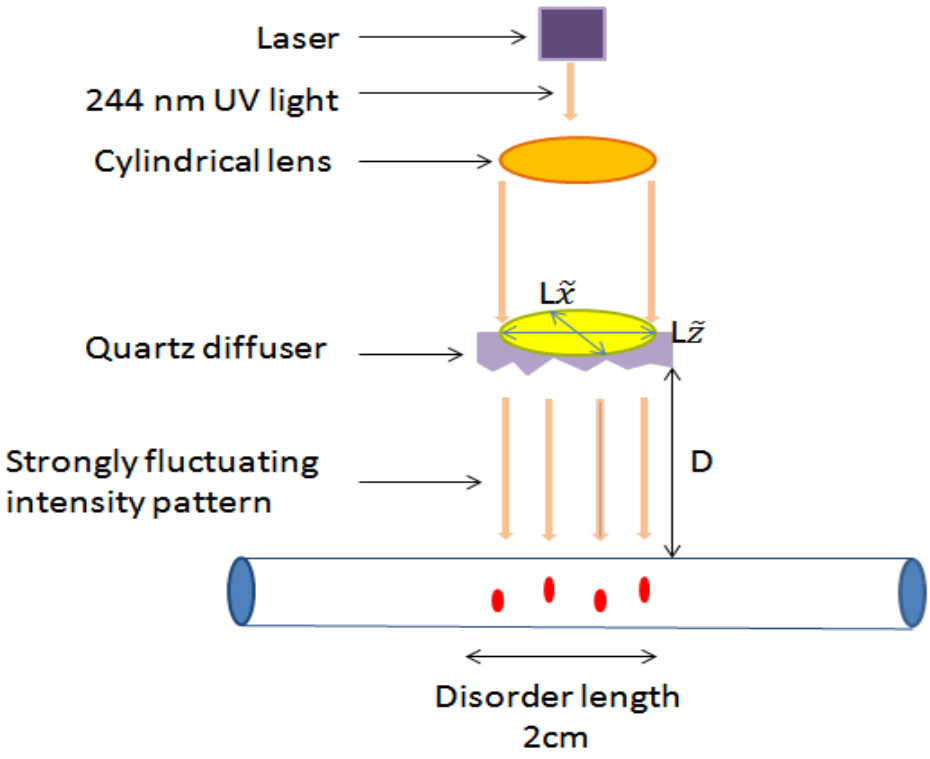

Figure 1.6: Schematic diagram of the experimental setup.

in the fabrication process. Hence, theoretical study starts with the microscopical model of photo-induced refractive index change introduced by Kamal and Russell [34]. Statistical properties of disorder are determined by those of the UV light's electric field. Expressions for the photo-induced change in both the dielectric tensor and its fluctuations are obtained with the Rayleigh-Sommerfield theory [39].

Once the statistical properties are found, the light propagation in the disordered fiber can be described theoretically. A new hybrid theory that combines coupled-power with coupled-mode approaches is derived for this purpose.

1.3.1. Hybrid Coupled-Power/Coupled-Mode Theory. The coupled-mode theory has been highly successful in describing properties of ordinary optical fibers [40]. Any deviation from the perfect order can potentially lead to coupling of

Figure 1.7: Optical transmission measurement. A linearly-polarized light is launched into the artificially disordered fiber. The output light is detected and analysed seperatly for X and Y polarizations.

the modes and, hence, to a transfer of power from one guided mode to another, as well as to the radiative modes.

The coupled-mode equations determine the amplitudes of all modes at a point z along the wave guide. They can be written in the following form:

$$\frac{dc_\nu(z)}{dz} = \sum_{\nu'} \mathcal{K}_{\nu\nu'}(z) c_{\nu'}(z) e^{i(\beta_\nu - \beta_{\nu'})z}, \tag{1.2}$$

where $c_\nu(z)$ is the amplitude at position z along the fiber, β_ν is the propagation constant, ν is the mode number, and $\mathcal{K}_{\nu\nu'}$ are the coupling coefficients. In this work, MMFs with artificial disorder support a relatively large number of modes (~ 20). Randomly varying coupling coefficients $\mathcal{K}_{\nu\nu'}$ induce both cross- and intra-polarization coupling between co-propagating modes. Although coupled-mode approach accounts for all possible interactions between the modes with both polarizations, it is impractical for describing the random coupling between large number of modes.

In this work, modal coefficients $c_\nu(z)$ are separated into two terms: (i) deterministic component $\langle c_{\nu,i}(z) \rangle$ which is treated via coupled-mode approach, and (ii) random component $\delta c_{\nu,i}(z) = c_{\nu,i}(z) - \langle c_{\nu,i}(z) \rangle$ described using coupled-power

approach[40]. The new hybrid theory is developed by combining these two approaches. It is tested experimentally and is found to accurately describe the output of the fibers with the artificial disorder.

1.4. OUTLINE OF THE DISSERTATION

In this dissertation, each chapter has been published as a journal article. Each chapter has an abstract, a introduction and a conclusion. The papers I and III describe the experimental procedure, demonstrate an efficient mode mixing and introduce a practical approach to control the statistical properties of the photo-induced fluctuations of the dielectric constant. The scalar theory theory presented in paper I describes the polarization-insensitive experiments without account of birefringence. In the paper II, the detailed microscopical model describing the changes in the susceptibility tensor during the process of fabricating the artificially disordered fiber is developed. In addition, paper II reports the statistical analysis of the light transmission through the disordered fiber. It describes the transient process of de-polarization of the light launched in to such fibers. The predictions of the theory are corroborated by the polarization-resolved experiments.

PAPER

I. FABRICATION, CHARACTERIZATION AND THEORETICAL ANALYSIS OF CONTROLLED DISORDER IN THE CORE OF OPTICAL FIBERS

[1]*N. P. Puente,* [2]*E. I. Chaikina,* [3] *S. Herath and* [3]*A. Yamilov*

[1]*Facultad Ingenieria-Ensenada, Universidad Autonoma de Baja California, Ensenada, B.C., 22860, México*

[2]*División de Física Aplicada, Centro de Investigación Científica y de Educación Superior de Ensenada,B.C., 22860, Ensenada, México*

[3]*Department of Physics, Missouri University of Science & Technology, Rolla, MO 65409*

ABSTRACT*

We present results of experimental and theoretical studies of polarization-resolved light transmission through optical fiber with disorder generated in its germanium-doped core via UV radiation transmitted through a diffuser. In samples longer than

*Published in Applied Optics **50** 802 (2011).

certain characteristic length, the power transmitted with preserved polarization is observed to be distributed over all forward-propagating modes as evidenced by the Rayleigh negative exponential distribution of the near-field intensity at the output surface of the fiber. Furthermore, the transmitted power becomes also equally distributed over both polarizations. To describe optical properties of the fibers with the experimentally induced disorder, a theoretical model based on coupled mode theory is developed. The obtained analytical expression for the correlation function describing spatial properties of the disorder shows that it is highly anisotropic. Our calculations demonstrate that this experimentally controllable anisotropy can lead to suppression of the radiative leakage of the propagating modes so that inter-mode coupling becomes the dominant scattering process. The obtained theoretical expressions for the polarization-resolved transmission fit very well the experimental data and the information extracted from the fit shows that radiative leakage is indeed small. The reported technique provides an easy way to fabricate different configurations of controlled disorder in optical fibers suitable for such applications as random fiber lasers.

1. INTRODUCTION

In recent years, there has been a considerable interest in optical disordered media. This is largely due to the new functionalities brought about when disorder is introduced into a homogeneous and periodic systems. A random laser[41], where laser action is ensured by coherent feedback in disordered structures, such as powders or porous crystals, is a striking example of this. In the paper [21] the advantages of disordered systems in wireless communications of high information capacity have been shown. It has also been reported [42] that the disorder induced in nonlinear crystals can greatly improve the efficiency of operation of nonlinear optical devices. It appears that disordered media open numerous possibilities for applications in sensors, nano-photonics and, more generally, in various light transmission systems.

Localization of electromagnetic radiation in strongly disordered random media has attracted great interest from both fundamental and practical points of view [43]. Studied in the optical as well as in the microwave spectral regions, the phenomenon of localization depends on the dimensionality of the system. In particular, in surface- [44] [45] and volume- [46] disordered waveguides it leads to arbitrarily small transmission, which diminishes exponentially with the length of the system. This disorder-induced confinement can be employed in such an application as a laser.

Disorder-induced confinement has been shown to lead to unusual while at the same time useful properties in photonic-crystal waveguides [47] and in optical fibers [48],[49],[50],[51],[52]. An optical fiber is an extremely promising experimental system for random lasing applications[53]: Lizárraga *et al.*[54] reported coherent random lasing on randomly distributed Bragg gratings in single mode optical fibers, whereas Turitsyn *et al.* [52] demonstrated an incoherent random lasing.

In this report we present experiments on the fabrication of random variations of the refractive index throughout the core of a Ge-doped multi-mode optical fiber,

whose parameters can be controlled in our experimental setup. The characteristics of the disorder created are evaluated from an analysis of the intensity distribution of the near-fields at the output of the fiber and by the analysis of the speckle size dependence of the total intensity of the transmitted light. The experimental results are compared, and agreement is found, with the predictions of the coupled mode theory, which is adapted to the particular type of volume disorder considered in this work. We show that the by varying the correlation size of the disorder, scattering sufficiently strong to achieve the complete mixing of the forward propagating modes can be achieved in a short centimeter-length segment of a multi-mode fiber. We also demonstrate that disorder with strongly anisotropic correlation function can lead to a dramatic suppression of radiative losses, so that coupling between modes becomes dominant. Thus, the scattering is much more efficient compared to the weak scattering off the material impurities as in, e.g. Ref. [52], and, unlike Bragg gratings, it is broad-band in propagation constant of a mode or the frequency of the light. The above properties of our system make is a promising candidate for fabrication of a compact multi-mode random fiber laser. This can be achieved by sandwiching the disordered segment of the fiber between two Bragg gratings which would provide a feedback.

The paper consists of the following sections. In Section 2 the experimental setup used for the fabrication of the fiber samples with disorder is described. In Section 3, one can find the experimental and numerical results on the intensity distribution of the light emerging from an optical fiber with different scales of the disorder. In Section 4 theoretical analysis of the optical properties of a fiber with speckled perturbations of the refractive index in its core is presented. Finally, discussion and the outlook are presented in Section 5.

2. FABRICATION OF THE DISORDER

The experimental setup utilized for the fabrication of disorder in optical fibers is schematically depicted in Fig. 1. In our experiments we employed a step-index optical fiber (PS1250/1500 of Fibercore) sensitized by Ge. The main parameters of the fiber are: the core diameter is 7.66 microns, the cladding diameter is 125 microns, and the numerical aperture (NA) NA $= 0.13$ with the refractive indices of the core and the cladding 1.463 and 1.457, respectively. The cutoff wavelength of the fiber with these parameters is about 1200 nm. The disorder was introduced in the Ge-doped fiber core by exposing it to UV light from an intracavity frequency doubled Argon-ion laser (244nm) which passed through a cylindrical lens and a diffuser, creating, in this way, a speckle pattern in a plane parallel to the fiber axis. The light beam generated by the UV laser was initially expanded by a cylindrical lens with a focal length 12 cm in order to form an elliptical spot with desired dimensions at the diffuser plane. The beam transmitted through the diffuser was used for exposing the photo-sensitive fiber. Speckle, as the strongly fluctuating, grainy intensity pattern resulting from the interference of randomly scattered coherent waves, resulted in fluctuations of the illuminating UV intensity in the fiber core. An expression for the size of a speckle, Eqs. (1.6)-(1.8) is derived in Sec. 4 below. It depends on the distance between the diffuser and the fiber axis, D, the size of the illuminated region in the diffuser plane $L_{x,z}$, and the wavelength of the recording UV light λ_{UV}. Variations of D in the range $2-8$ mm and of $L_{x,z}$ in the range of 8-10 mm allowed us to obtain an average speckle size along the fiber axis between 200 and 600 nm.

The length of each segment with the fabricated disorder was 1-2 cm. The experimental geometry allowed us to record the segments with lengths up to 5 cm. In order to achieve disorder with similar statistical parameters in each segment, the same exposure time was used for all segments, namely, about 10 minutes at a mean

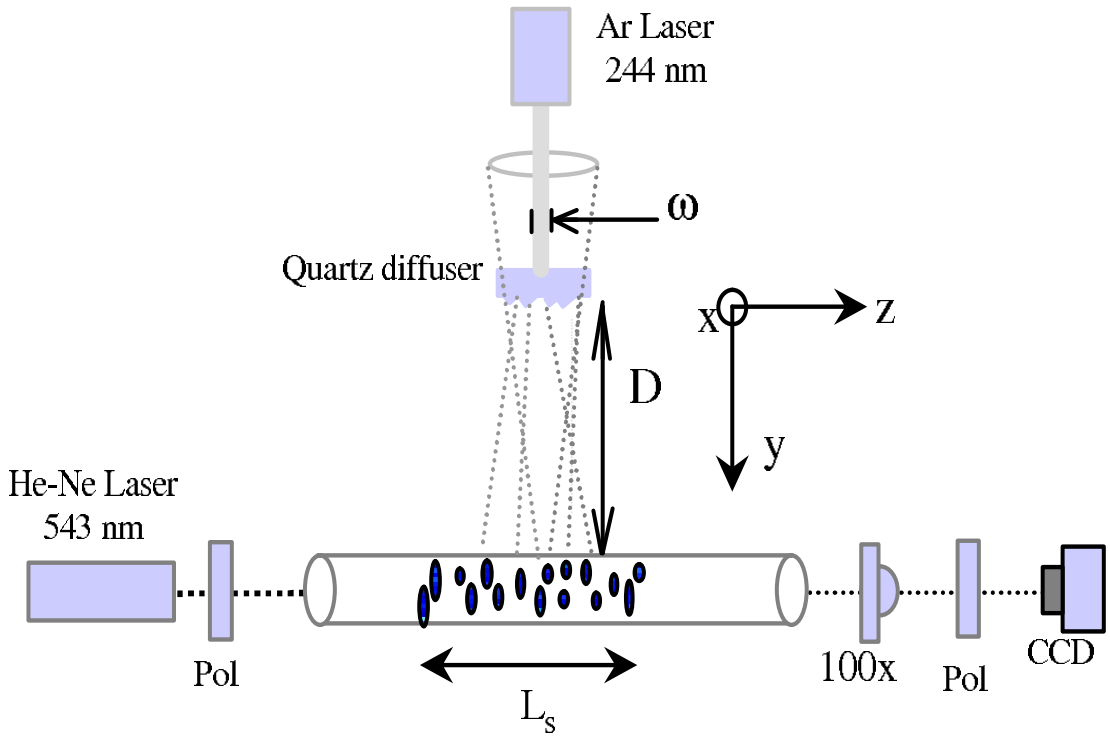

Figure 1: The experimental setup.

power of the UV laser of about 100 mW. We observed experimentally that after this exposure the intensity distribution of the output probe light at the fiber output did not change. Every next segment with a random distribution of the refractive index was recorded directly after the preceding one. The total lengths of the fabricated disordered part (L_s) were 2, 4, 6, 8, 10 and 15 cm.

After forming the disordered segment we launched the probe beam of the He-Ne laser operated at $\lambda = 543$ nm into the fiber, and detected the image of the output intensity distribution by a CCD camera (ST-402ME SBIG). The selected wavelength 543 nm of the probe beam ensured a low mode-number propagation regime, and corresponded to the sensitivity range of the CCD camera quite well. The light emerging

from the fiber passed through the microscope objective x100, which imaged the output end of the fiber on the CCD camera. In front of the CCD camera there was a polarizer utilized for characterization of the transmitted light.

3. EXPERIMENTAL RESULTS

The resulting V parameter of the utilized fibers was 5.8171 at the probe wavelength, and the expected number of the guided linearly polarized modes is $N = 20$. By varying the angle of incidence of the probe beam, different combinations of modes were excited and the corresponding near-field transmitted intensity was recorded. It appears that these measurements can be made quite reliably. Indeed, (i) the light polarization was preserved in the straight fiber without disorder; (ii) the ambient temperature was controlled be special air condition system that excluded the fluctuation of the parameters of the fiber samples during measurements. At the input of the optical fiber, the polarized light goes through a half wave-plate and a linear polarizer. The output light was detected separately for both polarizations: a) after passing through a polarizer of the same orientation as at the input (pp - polarization), or b) perpendicularly polarized (ps - polarization). We analyzed the output light of each polarization independently. The polarization extinction ratio of the laser source and the fiber output was measured in the linear transmission regime.

Examples of the intensity distribution of the light emerging from the fiber, obtained for different realizations of the disorder and for different angles of the incident beam with disordered segments of the fiber of 1 cm (a) and 2 cm (b) length, are presented in Fig. 2. The left column presents results of pp-polarization measurements, the right column presents results of ps - polarization measurements. Different realizations were obtained by slightly bending the disordered part of the fiber.

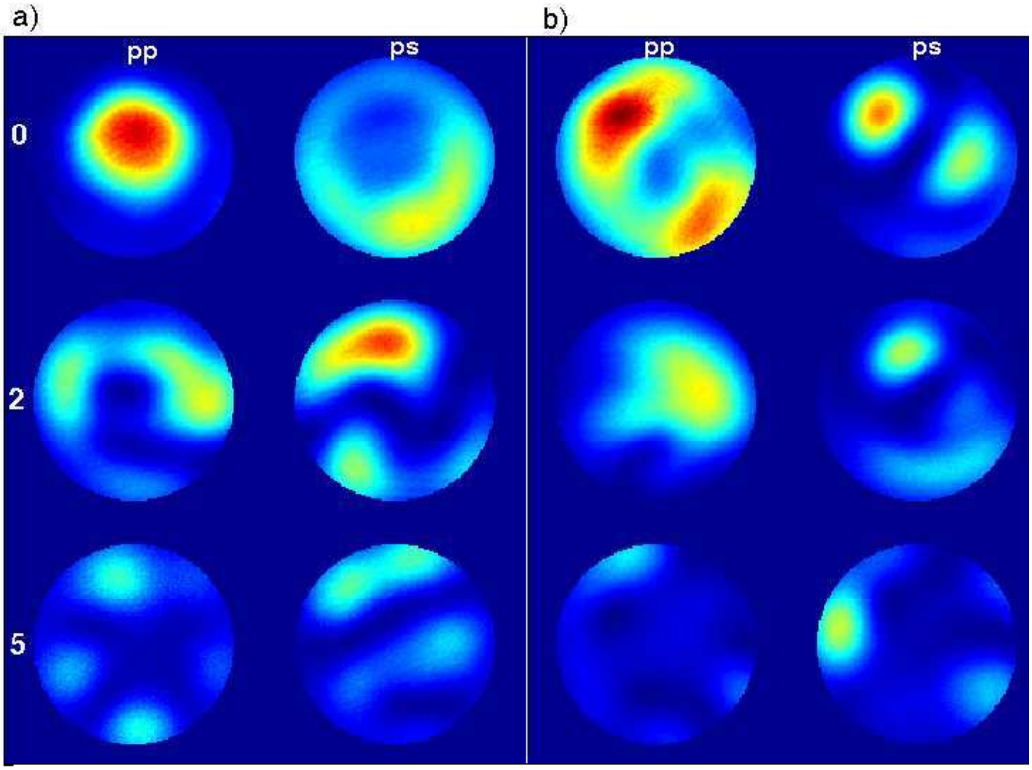

Figure 2: Examples of the output intensity distribution observed in some realizations with the disordered part of the fiber 1 cm (a) and 2 cm (b). The left column in each figure presents pp - polarized distribution, and the right column presents the ps - polarized one. The angles of incidence are 0°, 2° and 5° from the top to the bottom images.

In Fig. 3 the ensemble averaged intensities of the output light measured experimentally as functions of the length of the disordered parts of the fiber are presented. The averaging was performed over ten realizations. The solid and dashed lines are the fit with the theoretical expression Eqs. (1.24,1.25) obtained from Eq. (1.19) in the next section. The theoretical and experimental results show excellent agreement.

4. COUPLED-MODE THEORY IN FIBERS WITH SPECKLED PERTURBATIONS OF REFRACTIVE INDEX

As is shown in Sec. 3, the random fluctuations of refractive index imprinted in the core of the photo-sensitive fiber result in mixing of different forward propagating

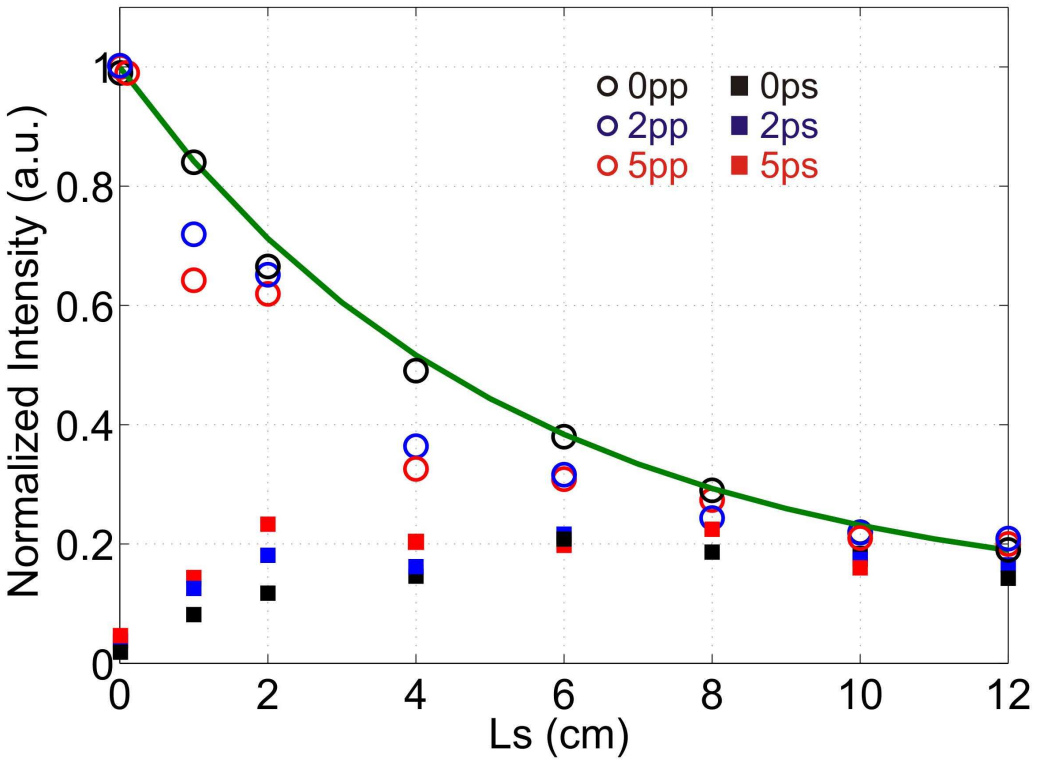

Figure 3: Experimentally measured total co- (open symbols) cross-polarized (solid symbols) transmission as a function of the length of the disordered part of the fiber for different polarization of the transmitted beam. The circles correspond to an angle of incidence of 0°, the triangles to 2°, and the squares to 5°. Solid and dashed lines represent the theoretical fit with Eqs. (1.24,1.25) with parameters $\alpha = 0.064cm^{-1}$, $\sigma_2 = 0.1917cm^{-1}$.

modes. To describe this process and to obtain the characteristic (mixing) length of the disordered segment of fiber, we employ the coupled-power method developed by Marcuse [40]. However, because the disorder induced by the speckle pattern, see Sec. 3, does not allow a factorization of the refractive index modulations into a product of a function of the transverse coordinates and a function of the longitudinal coordinate $\delta n(x, y, z) \neq \delta n(x, y) \times f(z)$, the original derivation is not applicable. The goal of this section is to obtain a system of coupled-power equations applicable to the experimentally induced disorder. In process of derivation we verify that coupling between the forward and backward propagating modes is negligible. We also give

detailed estimates of the radiative loss due to scattering into non-guiding modes. We show that because of the highly asymmetric correlation function of the disorder, the radiative loss is greatly reduced so it becomes comparable to the coupling coefficients between guided modes.

4.1. Statistical Properties of Disorder. To begin our analysis, we need to obtain the statistical properties of the disorder, specifically, the two-point correlator of the fluctuations of the dielectric function $\langle \delta\varepsilon(\mathbf{r})\delta\varepsilon(\mathbf{r}')\rangle$, where the angular brackets denote averaging over different realizations of disorder. Here we defined the fluctuation of the dielectric function $\delta\varepsilon(\mathbf{r}) = \varepsilon(\mathbf{r}) - \langle\varepsilon(\mathbf{r})\rangle$, which has the property $\langle\delta\varepsilon(\mathbf{r})\rangle = 0$. We make an assumption that in the process of exposure to the ultra-violet (UV) radiation the material in the fiber core remains in a linear regime, i.e.

$$\langle \delta\varepsilon(\mathbf{r})\delta\varepsilon(\mathbf{r}')\rangle = \langle\delta\varepsilon^2\rangle \frac{\left|\langle \mathbf{A}(\mathbf{r})\mathbf{A}^*(\mathbf{r}')\rangle\right|^2}{\langle|\mathbf{A}(\mathbf{r})|^2\rangle\langle|\mathbf{A}(\mathbf{r}')|^2\rangle} \equiv \langle\delta\varepsilon^2\rangle \left|\mu(\mathbf{r}',\mathbf{r})\right|^2, \tag{1.1}$$

where $\mathbf{A}(\mathbf{r})$ are statistically uniform complex field amplitudes of the UV light scattered by the diffuser. The amplitudes can be computed in the paraxial approximation with the help of the Fresnel diffraction integral which propagates the fields delta-correlated in the plane of the diffuser; the procedure is described in Sec. 4.4 of Ref. [55]. In our problem we are interested in $\langle \delta\varepsilon(\mathbf{r})\delta\varepsilon(\mathbf{r}')\rangle$ as a function of all three spatial coordinates, including both those perpendicular (x- and z-axes) and parallel (y-axis) to the direction of the UV illumination. In the geometry considered it is impossible to obtain such an expression in a compact form. To proceed we assume that

$$\mu(\mathbf{r}',\mathbf{r}) \approx \mu(\mathbf{r}'-\mathbf{r}) \approx \mu(x-x',0,z-z')\mu(0,y-y',0). \tag{1.2}$$

In this expression the first factor describes the correlation in the plane perpendicular to the UV propagation whereas the second factor describes the depth of the speckle. The expressions for these functions can now be computed with the knowledge that the gausssian UV laser beam is spread out by the cylindrical lens to cover the spot

$$I(\tilde{x},\tilde{z}) \propto \exp\left[-\tilde{x}^2/L_x^2 - \tilde{z}^2/L_z^2\right], \tag{1.3}$$

where $\tilde{x},\tilde{z}$ denote the coordinates in the plane of the diffuser. The intensity distribution in Eq. (1.3) allows one to compute the Fresnel integrals [55] which define the correlation functions $\mu(x-x',0,z-z')$ and $\mu(0,y-y',0)$ in Eq. (1.2). Performing the integrations we obtain

$$|\mu(x-x',0,z-z')|^2 = \exp\left[-\left(\frac{x-x'}{S_x}\right)^2\right] \times \exp\left[-\left(\frac{z-z'}{S_z}\right)^2\right] \tag{1.4}$$

$$\begin{aligned} |\mu(0,y-y',0)|^2 &= \frac{1}{\left(1+\left[\frac{\pi L_x^2}{\lambda_{UV}D^2}(y-y')\right]^2\right)^{1/2}\left(1+\left[\frac{\pi L_z^2}{\lambda_{UV}D^2}(y-y')\right]^2\right)^{1/2}} \\ &\approx \frac{1}{\left(1+\left[\frac{y-y'}{S_y^2}\right]^2\right)^{1/2}}. \end{aligned} \tag{1.5}$$

The length S_i were introduced to describe the spatial dimensions of the speckles:

$$S_x = \frac{\lambda_{UV}D}{\sqrt{2}\pi n_{core}L_x} \approx 0.15\frac{\lambda_{UV}D}{L_x} \tag{1.6}$$

$$S_y = \frac{\sqrt{3}\lambda_{UV} D^2}{\pi n_{core} L_z^2} \approx 0.38 \frac{\lambda_{UV} D^2}{L_z^2} \tag{1.7}$$

$$S_z = \frac{\lambda_{UV} D}{\sqrt{2}\pi n_{core} L_z} \approx 0.15 \frac{\lambda_{UV} D}{L_z}, \tag{1.8}$$

where D denotes the distance from the diffuser to the fiber core during the exposure; all dimensions are scaled by the refractive index of the core; and $L_z \gg L_x$ is assumed in Eq. (1.5). Finally, by substituting Eqs. (1.4,1.5) into Eq. (1.1), we obtain the sought expression for the second order statistics of disorder introduced in imprinting the speckle pattern in the core of the photo-sensitive optical fiber:

$$\langle \delta\varepsilon(\mathbf{r}) \delta\varepsilon(\mathbf{r}') \rangle \approx \langle \delta\varepsilon^2 \rangle \exp\left[-\left(\frac{x - x'}{S_x} \right)^2 \right] \frac{1}{\left[1 + \left(\frac{y - y'}{S_y^2} \right)^2 \right]^{1/2}} \exp\left[-\left(\frac{z - z'}{S_z} \right)^2 \right]. \tag{1.9}$$

The parameter $\langle \delta\varepsilon^2 \rangle = 2 n_{core} \Delta n_{UV}$ is related to the change in the refractive index Δn_{UV} due to the UV irradiation. We note that the above approximate expression remains valid for $|y - y'| \leq S_y$. For $|y - y'| \gg S_y$ the factor omitted in Eq. (1.5) has to be also included to ensure that the function is normalizable.

4.2. Derivation of Coupled-Power Equations. We begin our derivation of a system of coupled-power equations by expressing the electric field in terms of the linearly x- and y-polarized (LP) modes in the weakly guiding step-index fiber without disorder

$$\mathbf{E}(\mathbf{r}) \approx \sum_{\nu} c_\nu(z) e^{i(\omega t - \beta_\nu z)} \left(\mathcal{E}_{t,\nu}(x, y) + \hat{\mathbf{e}}_z \mathcal{E}_{z,\nu}(x, y) \right). \tag{1.10}$$

Here the summation runs over all modes ν of the fiber including the odd and even modes of both x- (odd ν's) and y-polarizations (even ν's), assumed to be normalized as

$$\beta_\nu \int\int \left[\mathcal{E}_{t,\nu}(x,y)\cdot\mathcal{E}_{t,\nu'}(x,y)\right] dxdy = \delta_{\nu\nu'}, \tag{1.11}$$

where $\delta_{\nu\nu'}$ is the Kronecker symbol. Eq. (2.13) contains contributions from only forward propagating modes. In Sec. 4.3 we will support this assumption by showing that the coupling coefficients into the backward propagating modes is negligible.

Further, in Eq. (2.13) the transverse $\mathcal{E}_{t,\nu}(x,y)$ and the longitudinal $\hat{\mathbf{e}}_z\mathcal{E}_{z,\nu}(x,y)$ components of the individual modes are retained despite the smallness of the latter. As will be seen below, retaining the longitudinal components is crucial because it gives the dominant contribution to the coupling between the modes with the orthogonal polarizations. β_ν is the propagation constant of the νth mode, and $c_\nu(z)$ is its amplitude at position z along the fiber.

Following [40], we obtain the coupled amplitude equation

$$\frac{dc_\nu(z)}{dz} = \sum_{\nu'} \mathcal{K}_{\nu\nu'}(z)c_{\nu'}(z)e^{i(\beta_\nu-\beta_{\nu'})z}, \tag{1.12}$$

where

$$\mathcal{K}_{\nu\nu'}(z) = \frac{\omega^2}{2c^2}\int\int \delta\varepsilon(\mathbf{r})\left[\mathcal{E}_{t,\nu}(x,y)\cdot\mathcal{E}_{t,\nu'}(x,y) + \mathcal{E}_{z,\nu}(x,y)\mathcal{E}_{z,\nu'}(x,y)\right] dxdy \tag{1.13}$$

are the amplitude coupling coefficients. The system of equations Eq. (1.12) can be used to obtain the solution for a particular realization of the random function

$\delta\varepsilon(\mathbf{r})$. The ensemble-averaged information can be obtained by defining the power in each mode as $P_\nu = \langle |c_\nu|^2 \rangle$ which satisfies the evolution equation

$$\frac{dP_\nu}{dz} = \langle c_\nu^* \frac{dc_\nu}{dz} \rangle + c.c.\,, \tag{1.14}$$

where c.c. stands for the complex conjugate. We proceed by substituting Eqs. (1.12,1.13) into Eq. (1.14). Evaluation of the ensemble average $\langle ... \rangle$ requires the following two assumptions. $\langle P_\nu(z) \rangle$ is assumed to vary on scales much larger than that of the disorder $S_z \sim \lambda$. This assumption is easily satisfied because the magnitude of the refractive index fluctuations is small – $\Delta n_{UV} \ll 1$. The experimental data in Fig. 3 further corroborates this assertion.

At this point, our derivation departs from that of Marcuse [40]. To evaluate $\langle |\mathcal{K}_{\nu\nu'}(z)|^2 \rangle$, instead of the stringent requirement that the function describing the disorder in the refractive index can be factorized as $\delta n(x,y,z) \neq \delta n(x,y) \times f(z)$, we use a much weaker assumption that z-dependence is factorizable in $\langle \delta\varepsilon(\mathbf{r}) \delta\varepsilon(\mathbf{r}') \rangle$. Indeed, the multiplicative property of the correlation in the speckle in Eq. (1.9) that separates the dependencies on the transverse (x and y) and the longitudinal (z) coordinates, enables one to complete the derivation of the system of coupled-power equations

$$\frac{dP_\nu}{dz} = \sum_{\nu'} h_{\nu\nu'} \left(P_{\nu'} - P_\nu \right) \tag{1.15}$$

with the power coupling coefficients given by the following expression

$$h_{\nu\nu'} = \langle \delta\varepsilon^2 \rangle \frac{\omega^4 \pi \log(2) S_x S_y S_z}{c^4} e^{-S_z^2 |\beta_\nu - \beta_{\nu'}|^2/4} \times \int\int \left[\mathcal{E}_{t,\nu}(x,y) \cdot \mathcal{E}_{t,\nu'}(x,y) + \mathcal{E}_{z,\nu}(x,y) \mathcal{E}_{z,\nu'}(x,y) \right]^2 dxdy \tag{1.16}$$

In obtaining Eq. (1.16),

We approximated $\exp\left[-\left(x-x'\right)^2/S_x^2\right] \times \left[1+\left(y-y'\right)^2/S_y^2\right]^{-1/2}$ by the product of two delta functions $4\pi^{1/2}\log(2)S_xS_y\delta\left(x-x'\right)\delta\left(y-y'\right)$ with the coefficients chosen so that both pairs of functions enclose identical area. This approximation is justified fairly well in our case because $S_{x,y}$ are smaller than the characteristic scale, a, of the field variation in the transverse direction for all guided modes. In case of the function that describes y-dependence, the full expression Eq. (1.5) was used to obtain the normalization and the correction terms logarithmic in L_x/L_z were omitted in the result.

4.3. Efficiency of Backscattering. In process of derivation of the coupled power equations Eqs. (1.15,1.16) we neglected the possibility of scattering from a forward propagating mode into one of the backward propagating modes. This is an important process which, if efficient, can give rise to the phenomenon of Anderson localization which originates in the studies of mesoscopic systems in condensed matter physics[56]. Multiple scattering and interference of the forward- and backward-propagating waves can suppress transmission and lead to an exponential decay of the transmission coefficient. This dependence may appear similar to that observed in Fig. 3.

To estimate the efficiency of the backscatering process in our system, we compute the forward-to-backward coupling coefficients. The derivation follows the steps similar to those in Sec. 4.2 with the final expression for $h_{\nu\nu'}^{+,-}$ being given by the formula similar to Eq. (1.16) with an exception that $\exp\left[-S_z^2\left|\beta_\nu-\beta_{\nu'}\right|^2/4\right] \simeq 1$ factor is replaced by $\exp\left[-S_z^2\left|\beta_\nu+\beta_{\nu'}\right|^2/4\right] \ll 1$. One can see that this difference, proves to be extremely important because $|\beta_\nu-\beta_{\nu'}| \ll |\beta_\nu+\beta_{\nu'}| \simeq 2n_{core}\times(2\pi/\lambda)$ and $S_z \lesssim \lambda$ in our fibers.

The above estimate shows that the backscattering mechanism is, indeed, strongly suppressed in the considered system as it was assumed in the previous section. As a consequence, we do not expect our system to exhibit the phenomenon of Anderson localization.

4.4. Radiative Losses. Optical fiber with unwanted or purposefully introduced, as in our case, modulations of the refractive index are invariably susceptible to the radiative losses. Indeed, the index nonuniformity couples the modes guided in the core of the fiber to the non-guided modes that extend into the cladding and are effectively lost. Even the fibers of the highest quality suffer from radiative loss from Rayleigh scattering on molecular inclusions introduced in its fabrication process[36]. The consequence of this loss is the exponential decay of the power in a mode $P_\nu(z) \propto \exp[-\alpha_\nu z]$. Unlike the losses suffered in waveguides with rough surfaces, the radiative loss in the volume-disordered fibers, such as fibers with molecular defects, should not exhibit a strong dependence on the mode index ν. Because the fibers studied in this work are of the latter kind, we will assume $\alpha_\nu \equiv \alpha$ hereafter.

In Chapter 4 of Ref. [40] Marcuse has derived an expression for α in case of Rayleigh scattering. It is interesting to note that under quite general conditions the ratio between coupling coefficients and the scattering loss appears to be independent of the disorder parameters[57]

$$\frac{\alpha}{h_{\nu\nu'}} \simeq \frac{2}{3\pi} k_0^2 n_{core}^2 A, \tag{1.17}$$

where $k_0 = 2\pi/\lambda$ and A is the area of the fiber core. One can easily see that the above estimate gives $\alpha/h_{\nu\nu'} \gg 1$ for a step index fiber with $(n_{core} - n_{cladding})/n_{core} \ll 1$. Evaluating this ratio for our system gives a number on the order of a thousand. Although the above estimate is made under assumption of Rayleigh scattering, it may still be applicable in our case. This is because the Rayleigh criterion involves

not only the smallness of the scatterer compared to the wavelength of light but also the difference between its refractive index and that of the surrounding [58]. Below, we expose a flaw in this logic and show that Eq. (1.17) is not applicable to our system and that instead $\alpha \sim h_{\nu\nu'}$

Unlike a deterministic scattering off a single particle, the scattering in a random system has to properly account for the exact autocorrelation function given in our system by Eq. (1.9). The combined effect for a group of scatters can be greatly diminished if the phases of the partial waves are sufficiently random. Quantitatively this effect is described [40] by the following integral

$$\alpha \propto I = \int d\Omega_{\Delta\mathbf{k}} \left(\hat{\mathbf{e}}_{scat} \cdot \hat{\mathbf{e}}_z\right)^2 \iiint_{-\infty}^{\infty} du_x du_y du_z \langle \delta\varepsilon(\mathbf{r}) \delta\varepsilon(\mathbf{r}+\mathbf{u}) \rangle \exp\left[i\Delta\mathbf{k} \cdot \mathbf{u}\right]. \quad (1.18)$$

Here, $\Delta\mathbf{k} \approx n_{core} k_0 \left(\hat{\mathbf{e}}_{scat} - \hat{\mathbf{e}}_z\right)$ defines the change of wave vector after scattering and $\int d\Omega_{\Delta\mathbf{k}} ...$ denotes the solid angle integration over all possible scattering directions.

Rayleigh approximation in Eq. (1.18) amounts to assuming that disorder is correlated in the volume L_{corr}^3 much less then λ^3, that results in $\exp\left[i\Delta\mathbf{k} \cdot \mathbf{u}\right] \simeq 1$. In the optical fibers with photo-induced disorder considered in our work, this assumption is no longer valid. Thus, Rayleigh result $I = (4\pi/3) \langle \delta\varepsilon^2 \rangle L_{corr}^3$ needs to be re-evaluated for the correlator Eq. (1.9) we obtained in Sec. 4.1.

Calculation of the triple integral in Eq. (1.18) is facilitated by the fact that $\langle \delta\varepsilon(\mathbf{r}) \delta\varepsilon(\mathbf{r}+\mathbf{u}) \rangle$ is factorizable into three functions each of which depend only on one spatial variable. The integrals over u_x and u_z give rise to $\sqrt{\pi} S_{x,z} \exp\left[-(\Delta k_{x,z} S_{x,z}/2)^2\right]$. The integral over u_y does not give, in general, a compact expression. However, in a special case when $L_x = L_z$ it leads to a simple expression which illuminates the general tendency: $\pi S_y \exp\left[-\Delta k_y S_y\right]$. Inspection of all three integrals shows that the result

of the triple integral in Eq. (1.18) is a function which is very strongly peaked around $|\Delta\mathbf{k}| = 0$. Therefore, the remaining integration over solid angles should produce the result much smaller then $4\pi/3$ predicted for the isotropic (Rayleigh) scattering. To complete our calculation of the absorption coefficient α we perform the integral over $d\Omega$ in Eq. 1.18 numerically and report the results in Fig. 7.

4.5. Solution of Coupled-Power Equations. The system of coupled-power Eqs. (1.15) obtained in Sec. 4.2 did not account for loss. This omission can be rectified by a phenomenological correction due Marcuse [40]

$$\frac{dP_\nu}{dz} = -\alpha P_\nu + \sum_{\nu'} h_{\nu\nu'} \left(P_{\nu'} - P_\nu\right) \tag{1.19}$$

Such a treatment of loss can be rigorously justified in the case when the such a loss is independent of the mode index [29]. As already mentioned in the preceding section, this a reasonable assumption for the volume disordered fibers that we also adopt here.

Solution of Eqs. (1.19) proceeds with two steps. First, the effect of the radiative loss is factored out with substitution

$$P_\nu(z) = P_\nu^{(lossless)}(z) \times \exp\left[-\alpha z\right], \tag{1.20}$$

which reduces Eqs. (1.19) back to Eqs. (1.15) satisfied now by $P_\nu^{(lossless)}(z)$.

In the second step, the solution for $P_\nu^{(lossless)}(z)$ is obtained by the following ansatz

$$P_\nu^{(lossless)}(z) = A_\nu \exp\left[-\sigma z\right], \tag{1.21}$$

where σ_n and the corresponding set of $A_\nu^{(n)}$ are to be determined by substitution of Eq. (1.21) into Eq. (1.15). Here σ_n are the eigenvalues of the secular equation

$$\det\left[h_{\nu\nu'} - \delta_{\nu\nu'}\sum_{\tau} h_{\nu\tau} + \sigma\right] = 0 \tag{1.22}$$

arranged in increasing order. The overall solution for $P_\nu(z)$ takes form

$$P_\nu(z) = e^{-\alpha z} \times \left[\sum_n c_n A_\nu^{(n)} e^{-\sigma_n z}\right], \quad \text{with} \quad c_n = \left[\sum_n A_\nu^{(n)} P_\nu(0)\right]. \tag{1.23}$$

Because the effect of radiative loss has been factored out in Eq. (1.20), the conservation of the total power for $P_\nu^{(lossless)}$ requires $\sigma_1 \equiv 0$ and, subsequently, $A_\nu^{(1)} = const = 1/N$ leads to uniform distribution of the power over all modes. The knowledge of σ_n allows estimation of the characteristic lengths of the disordered region of the fiber beyond which such asymptotic state is achieved, $\ell^{(xx)} \equiv \sigma_3^{-1}$, and for cross-polarized modes, $\ell^{(xy)} \equiv \sigma_2^{-1}$. Assuming that the fiber is excited with some mode combination (with total input power equal to unity) of the same polarization, which we assume to be x for definitiveness, and recalling mode numbering convention in Eq. (2.13) we obtain

$$P^{(x)}(z) \equiv \sum_{\nu=0}^{N/2-1} P_{2\nu+1} \approx e^{-\alpha z} \times \frac{1}{2}\left[1 + e^{-\sigma_2 z}\right], \tag{1.24}$$

$$P^{(y)}(z) \equiv \sum_{\nu=1}^{N/2} P_{2\nu} \approx e^{-\alpha z} \times \frac{1}{2}\left[1 - e^{-\sigma_2 z}\right]. \tag{1.25}$$

The above equations have the following properties. Without loss and polarization coupling, $P^{(x)}(z) = 1$ reflects power conservation. In the presence of absorption $P^{(x)}(z) + P^{(y)}(z) = \exp[-\alpha z]$ exhibits attenuation due to the radiative losses.

In the case when coupling between two orthogonal subsets of LP modes of the fiber is weak, $\sigma_2 \ll \alpha \ll \sigma_3$, Eq. (1.23) yields $P^{(y)}(z) \sim 0$, $P^{(x)}(z) \simeq \exp[-\alpha z]$ and

the system reaches the state when the power is equally distributed only over $(N/2)$ modes with initially excited polarization, x:

$$P_{2\nu+1}(z) \approx e^{-\alpha z} \times \left[\left(P_{2\nu+1}(0) - \frac{2}{N} \right) e^{-\sigma_3 z} + \frac{2}{N} \right], \quad P_{2\nu}(z) \sim 0. \tag{1.26}$$

The above analysis shows that the redistribution of the power carried by the forward propagating modes can be detected by making the following observations:

- Making polarization-resolved measurement of the light intensity at the output surface of the fiber and averaging it over several disorder configurations should show that intensity profile approaches the limit. Alternatively, the conclusion that a perfect mixing (in a statistical sense, i.e. $P_\nu(z \to \infty) \to const$) indeed occurs in our experimental system can also be tested through measurements of the distribution of the near-field intensity at different spatial locations for just one realization of disorder. A random sum of different modes of the fiber $\sum_\nu c_\nu \mathcal{E}_{t,\nu}(x,y)$ with $P_\nu \approx const$ is expected [55] to result in the Rayleigh negative exponential distribution of the intensity. In an optical fiber, however, the coefficients c_ν are not completely random because the total power carried by all modes is constrained by $\sum_\nu |c_\nu(z)|^2 = \exp[-\alpha z]$. This constraint, similar to the power conservation in the lossless fibers [37], makes the distribution deviate slightly from the Rayleigh form. As can be seen from Fig. 4, the agreement between theory and experiment is very good, whereas the level of precision of the experimental data does not allow distinguishing between the two theoretical functions – unconstrained and constrained random sums of all modes of the fiber.

- The dependence of $P^{(x)}(z=L_s), P^{(y)}(z=L_s)$ on the length of the disordered segment of the fiber, L_s, is expected to be described by Eqs. (1.24,1.25). We observe that the power carried by a particular mode ν, $P_\nu = \beta_\nu \int\int [\mathcal{E}_{t,\nu}(x,y)\cdot\mathcal{E}_{t,\nu'}(x,y)]\,dxdy$ is equal to the product of nearly ν-independent $\beta_\nu \approx n_1 k_0$ and the field intensity integrated over the surface of the fiber $\mathcal{I}$. Therefore, even in case of superposition of several modes with the same polarization, the area-integrated intensity at the output fact, $\mathcal{I}^{(x,y)} = \int\int \left|\sum_\nu c_\nu \mathcal{E}_{t,\nu}^{(x,y)}(x,y)\right|^2 dxdy = \sum_\nu \int\int |c_\nu|^2 \left|\mathcal{E}_{t,\nu}^{(x,y)}(x,y)\right|^2 dxdy \approx (1/n_1k_0)\sum_\nu P_\nu^{(x,y)}$ is proportional to $P^{(x)}(z)$ and $P^{(y)}(z)$ given by Eqs. (1.24,1.25). The outcome of the fit by these expressions to the experimental data in Fig. 3 allows one to extract the characteristic mixing length $\ell^{(xy)} = \sigma_2^{-1}$ and loss coefficient α.

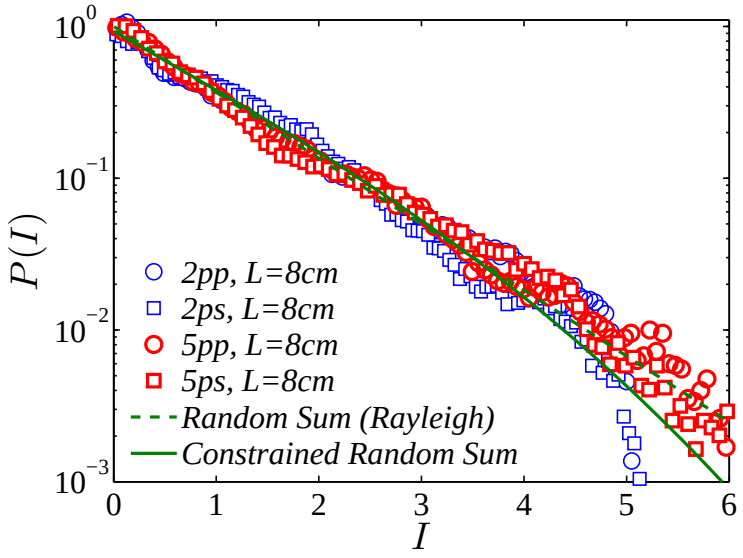

Figure 4: The distributions which correspond to an unconstrained random sum (shown as a dashed curve) and to a constrained random sum (shown with the solid line) of all modes of the fiber, are compared to the experimentally observed distributions of the near-field intensity measured in co- (circles) and cross-polarized (squares) channels in a sample with L=8cm. The thin symbols correspond to an angle of incidence of 2°, and the bold ones to an angle of incidence of 5°.

Approximate expressions for the mixing lengths can be obtained in a compact analytic form by taking into account the fact that both the transverse $\mathcal{E}_{t,\nu}(x,y)$ and the longitudinal $\hat{\mathbf{e}}_z\mathcal{E}_{z,\nu}(x,y)$ modal profiles are spread out over the entire core of the fiber. This observation together with Eq. (1.11) allows one to estimate

$$\int\int \left[\mathcal{E}_{t,\nu}(x,y)\cdot\mathcal{E}_{t,\nu'}(x,y)+\mathcal{E}_{z,\nu}(x,y)\mathcal{E}_{z,\nu'}(x,y)\right]^2 dxdy \tag{1.27}$$

$$\approx \begin{cases} \left[n_{core}^2(\omega^2/c^2)\pi a^2\right]^{-1} & xx,\ yy \\ (NA/2)^4\left[n_{core}^2(\omega^2/c^2)\pi a^2\right]^{-1} & xy,\ yx\,. \end{cases} \tag{1.28}$$

where a is radius of the fiber core. In the second case of the cross-polarized modes we also used the fact that the amplitude of the $\mathcal{E}_{z,\nu}(x,y)$ component is a factor $NA/2$ smaller compared to the amplitude of the transverse fields. The approximations in Eq. (1.28), $\sigma_{2,3}\sim h_{22,33}$ and $S_z\left|\beta_\nu-\beta_{\nu'}\right|\ll 1$ allow us to obtain our final result in a closed analytical form

$$\begin{aligned} \ell^{(xx)-1}\equiv\sigma_3 &\sim \frac{\Delta n}{2n_{core}}\frac{\pi\omega^2 S_x S_y S_z}{c^2a^2}=\frac{\Delta n}{n_{core}^4}\frac{\lambda_{UV}^3 D^4}{\lambda^2 a^2 L_x L_z^3}, \\ \ell^{(xy)-1}\equiv\sigma_2 &\sim \ell_{mixing}^{(xx)-1}\left(\frac{NA}{2}\right)^4, \end{aligned} \tag{1.29}$$

where Eqs. (1.6)-(1.8) were used.

In Fig. 5 we plot the dependence of the speckle size as a function of the distance D between the diffuser and the fiber core. It is clear that tuning this parameter allows one to widely tune the characteristic size of the prepared disorder. This is an attractive feature of the fabrication technique described in Sec. 2.

In Fig. 6 three expressions for $\ell^{(xx)}$ obtained in this section are compared. As expected, for small speckle size (small D), the approximation of Eq. (1.9) by a

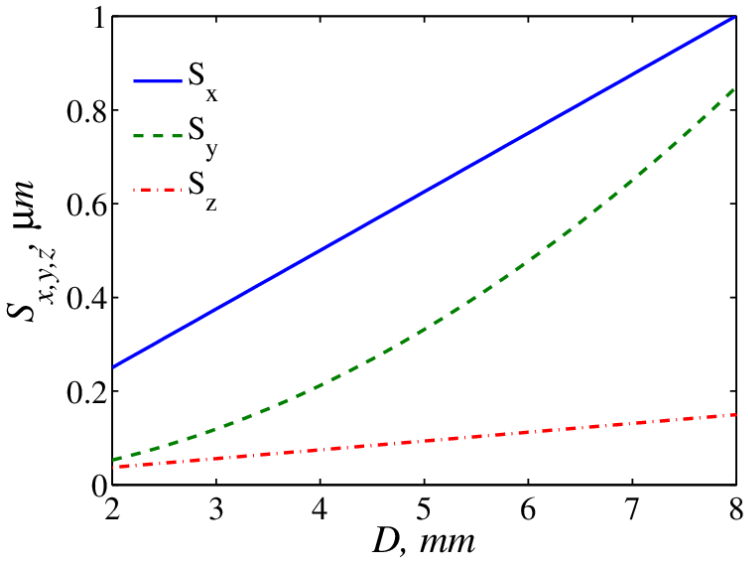

Figure 5: The size of the speckle defined by Eqs. (1.6)-(1.8) with $L_x = 0.3mm$ and $L_z = 2mm$ as a function of the distance between the diffuser and the core of the photo-sensitive fiber.

product of delta functions appears to be justified and gives a quite accurate result when compared to the direct numerical evaluation of $h_{\nu\nu'}$.

Numerical evaluation of the exact expressions in Eq. (1.16,1.22) with the experimentally relevant parameters ($L_x = 0.5mm$, $L_z = 3mm$ and $D = 0.5cm$) yields $\sigma_3 = \ell^{(xx)-1} \simeq 0.15cm^{-1}$, $\sigma_2 = \ell^{(xy)-1} \simeq 3\times10^{-6}cm^{-1}$, and $\alpha \simeq 0.015cm^{-1}$,see Fig. 7.

5. CONCLUSIONS

We have studied the transmission of light through a volume disordered multimode optical fiber. The disorder was introduced in the germanium-doped core of the fiber via UV radiation transmitted through a diffuser. The disorder generated in an optical fiber can be controlled by the experimental conditions, and is determined by the speckle size and the value of the induced difference in refractive index. The measurement of the transmission as a function of the length of the disordered section demonstrates the uniform distribution of the power over all forward-propagating

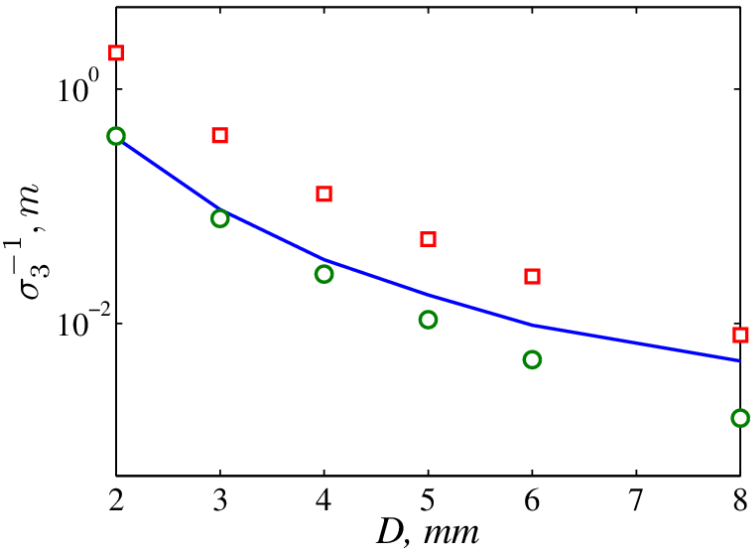

Figure 6: Compares the values of the characteristic length $\ell^{(xx)-1} \equiv \sigma_3$ after which all forward propagating modes with one polarization become equally populated. It is found numerically from Eq. (1.16) without (solid line) and with (circles) the delta function approximation to the order of magnitude estimate (squares) in Eq. (1.29).

modes beyond $L_s = 15cm$. For long sections of a disordered fiber, the experimentally measured distribution of the near-field intensity at the output surface of the fiber is well described by the Rayleigh negative exponential function. The presented technique provides an easy way to fabricate different configurations of controlled disorder in optical fibers suitable for applications as a coherent and incoherent random fiber laser. Although the specific type of disorder studied in our work leads to mixing of only forward-propagating modes, the feedback necessary to produce laser action can be achieved by surrounding the disordered fiber with Bragg gratings.

Analysis of Fig. 3 shows that the power transfer into the cross-polarized modes occurs quite efficiently with $\ell^{(xy)} \simeq \ell^{(xx)}$. This differs from the predictions of the coupled mode theory developed in Sec. 4 that gives $\ell^{(xy)} \gg \ell^{(xx)}$. We attribute this enhanced cross-polarization coupling to (i) birefringence effect induced by the bending of the fiber, and (ii) strongly anisotropic disorder pattern defined by Eq. (1.9). Indeed,

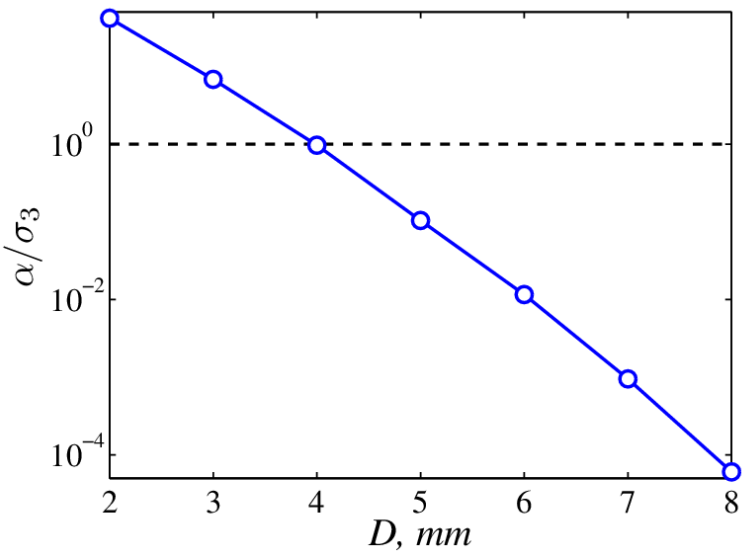

Figure 7: Compares the amplitude of the radiative loss rate computed from Eq. (1.18) to the inter-mode coupling rate σ_3. The plot shows that for the disorder patterns generated with $D > 4mm$ the coupling becomes dominant effect. This conclusion is borne out by the experimental results in Fig. 3.

although no polarization mixing is observed in the blank fibers (before the disorder is introduced), to generate the statistical ensemble of different realization, the 30-cm long fiber sample was displaced in lateral directions, while both of the sample's ends were fixed by fiber clips. As a result of fiber bending and tension, a pronounced birefringence was induced. For our experimental condition we estimate the minimum radius of the bending as 250 cm, which gives birefringence $\Delta n \sim 4 \times 10^{-5}$ [59]. Formally, the induced birefringence enables coupling via the transverse components of the modes field, that is expected to remove the small factor $(NA/2)^4$ which lead to $\ell^{(xy)} \gg \ell^{(xx)}$ condition in Eq. (1.28). The effect of induced birefringence will be reported in a separate publication.

6. ACKNOWLEDGMENTS

We thank Professor A. A. Maradudin and Dr. E. R. Méndez for stimulating discussions and constructive comments to manuscript. NPP and EIC would like to acknowledge a support by CONACYT (México), under grant UCM-42127. The work at Missouri S&T was supported by the University of Missouri Research Board and by the National Science Foundation Grant No. DMR-0704981.

II. ARTIFICIALLY DISORDERED BIREFRINGENT OPTICAL FIBERS

[1] *S. Herath,*[2] *N. P. Puente,* [3] *E. I. Chaikina, and* [1] *A. Yamilov*

[1] *Department of Physics, Missouri University of Science & Technology, Rolla, MO 65409*

[2] *Universidad Autónoma de Nuevo León, UANL, FIME, Av. Universidad S/N Ciudad Universitaria San Nicolás de los Garza Nuevo León, C.P. 66451 México*

[3] *División de Física Aplicada, Centro de Investigación Científica y de Educación Superior de Ensenada,B.C., 22860, Ensenada, México*

ABSTRACT*

We develop and experimentally verify a theory of evolution of polarization in artificially-disordered multi-mode optical fibers. Starting with a microscopic model of photo-induced index change, we obtain the first and second order statistics of the dielectric tensor in a Ge-doped fiber, where a volume disorder is intentionally inscribed via UV radiation transmitted through a diffuser. A hybrid coupled-power & coupled-mode theory is developed to describe the transient process of de-polarization of light launched into such a fiber. After certain characteristic distance, the power is

*Published in Optical Express **20**, 3620-3632 (2012).

predicted to be equally distributed over all co-propagating modes of the fiber regardless of their polarization. Polarization-resolved experiments, confirm the predicted evolution of the state of polarization. Complete mode mixing in a segment of fiber as short as $\sim$ 10cm after $3.6dB$ insertion loss is experimentally observed. Equal excitation of all modes in such a multi-mode fiber creates the conditions to maximize the information capacity of the system under e.g. multiple-input-multiple-output (MIMO) transmission setup.

1. INTRODUCTION

The last decade has witnessed a shift in the general perception of disorder in optical systems from a nuisance [60] to an exploitable feature which may enable some unique functionalities [32, 42, 61, 62, 63]. An ability to control light propagation in complex media [62] via spatial light modulator (SLM) exposed a deep connection to the problem of time reversal in acoustics [64] and renewed interest in such systems. SLM has also been used to manipulate certain aspects of propagation, e.g. to compensate modal dispersion, in multi-mode optical fibers MMF [19, 65].

Mutiple-input-multiple-output (MIMO) approach [9, 10, 21] has become the backbone of the wireless IEEE 802.11n standard for local area networks (LANs). It takes advantage of the differences in propagation from multiple sources to multiple receivers to maximize the bandwidth of the transmitted signal – with the theoretical limit of improvement over single-input-single-output (SISO) being proportional to number of sources or receivers, whichever is smallest [10].

A similar approach has also been applied to MMF [11]. It relies on the modal-coupling diversity (MCD) to take advantage of all available degrees of freedom in a MMF. Importantly, the method does not require orthogonal coupling to the individual modes of the fiber and its effectiveness is not degraded by inter-mode coupling in the fiber [66, 67]. To maximize MCD, the mode coupling coefficients in the fiber link should be sufficiently random – Gaussian [10, 22]. In conventional fibers, meeting this condition requires sufficiently long segments of MMF because concentration of imperfections is low. In the most disordered case of plastic optical fibers (POF) the characteristic length for mode mixing is on the order of $\sim$ 10m [32]. Improving the efficiency of inter-mode coupling and randomization by increasing the concentration of defects has the drawback of enhanced losses.

In this work we investigate both theoretically and experimentally photo-sensitive multi-mode Ge-doped silica fibers with artificially induced disorder. Our thorough account of the photo-induced birefringence allows us to develop a theory which captures the effect of direct coupling between two sets of modes with both orthogonal polarizations. Experimental observations demonstrate that the transition to the fully mode-mixed state occurs in very short fibers of length $\sim 10cm$. Because of such short length of the fiber, other sources of birefringence can be neglected. Furthermore, it should be possible to mitigate the trade-off between strength of inter-mode coupling and the radiative losses by controlling spatial correlations of the disorder [68].

Coupled-power theory [40] has been widely used to describe the modal distribution, as well as the temporal characteristics of pulse propagation and pulse bandwidth [28, 32, 69]. However, power-coupling models fail to properly describe the effect of birefringence because the latter affects the amplitudes and phases of the cross-polarized modes. Here we develop a hybrid coupled-power/coupled-mode approach which shows that the limiting modal distribution is uniform – all co-propagating modes (including those with orthogonal polarization) of the MMF are statistically equally excited. This implies optimum MCD to maximize the information capacity in transmission through MMF. Moreover, the developed formalism allowed us to describe and interpret a crossover from an initial mode distribution to the limiting one.

2. PROPERTIES OF PHOTO-INDUCED DISORDER

2.1. Microscopic Model of Birefringence. Photo-sensitivity of the germano-silicate fibers [33] allows one to modify the refractive index in the core of optical fibers. This effect has been used to laser-write a wide variety of fiber gratings [35]. Doping by germanium atoms leads to oxygen-deficient defect formation. Illumination by

a UV source with a sufficiently short wavelength breaks these bonds that, in turn, modifies the absorption spectrum of the glass. The real part of the refractive index is changed through the Kramers-Kronig relation.

It has also been observed that under certain conditions the photo-modified fibers become birefringent. Three contributions to photo-induced birefringence have been identified: (i) a contribution which depends on the polarization of the UV laser source [34, 38]; (ii) a contribution due to spatial non-uniformity of the incident UV beam [70] ; and (iii) a contribution related to modification in glass stresses [71]. Commonly, the first contribution is the dominant one. A detailed microscopical model describing the dependence of the birefringence on the polarization state of the UV radiation was developed Kamal and Russell in Ref. [34].

The Kamal-Russell model relates the macroscopic change in the local susceptibility tensor $\Delta\chi_{ij}(\vec{r})$ to the change in the volume density of the highly directional breakable bonds $\Delta\rho(\vec{r},\theta,\phi)$ in the germano-silicate glass as

$$\Delta\chi_{ij}(\vec{r}) = \alpha_b \int \Delta\rho(\vec{r},\theta,\phi)\, u_i u_j d\Omega, \tag{2.1}$$

where α_b is the polarizability of the bond, $\vec{u} = (\sin\theta\cos\phi, \sin\theta\sin\phi, \cos\theta)$ define the orientation of the bond, and the integral is taken of over all solid angles Ω. The process of severing the bond is described by the Fermi golden rule with the dipole – electric field interaction Hamiltonian. The change $\Delta\rho(\vec{r},\theta,\phi)$ in the initially isotropically uniform distribution $\rho/(4\pi)$ is related to the cumulative effect of UV radiation during the time of the exposure. Photo-induced change in the susceptibility tensor is then related to the UV electric fields

$$\Delta\chi_{xx}(\vec{r}) = C_0\left[3\left|E_x^{(UV)}(\vec{r})\right|^2 + \left|E_y^{(UV)}(\vec{r})\right|^2 + \left|E_z^{(UV)}(\vec{r})\right|^2\right], \tag{2.2}$$

$$\Delta\chi_{xy}\left(\vec{r}\right)=C_0\left[E_x^{(UV)}\left(\vec{r}\right)E_y^{(UV)*}\left(\vec{r}\right)+E_x^{(UV)*}\left(\vec{r}\right)E_y^{(UV)}\left(\vec{r}\right)\right], \tag{2.3}$$

where C_0 encompasses all material-related parameters, not essential to the further discussion. The remaining components of the tensor are obtained from Eq. (2.2) and Eq. (2.3) via permutation of the subscripts. Using this result, in the next section we obtain the relationship between statistics of the speckle pattern of the incident UV light and the spatial correlation of the elements of the dielectric tensor.

2.2. Statistical Properties of the UV Light Used to Fabricate the Disorder. As we will see in the following sections, to describe coupling between different modes of our disordered fiber we need first to determine the spatial correlations of the random fluctuations of the dielectric tensor around its average $n_{core}^2+\langle\Delta\chi_{ij}(\vec{r})\rangle$

$$\langle\delta\epsilon_{ij}(\vec{r})\delta\epsilon_{ij}(\vec{r}')\rangle\equiv\langle(\Delta\chi_{ij}(\vec{r})-\langle\Delta\chi_{ij}(\vec{r})\rangle)\cdot(\Delta\chi_{ij}(\vec{r}')-\langle\Delta\chi_{ij}(\vec{r}')\rangle)\rangle\,. \tag{2.4}$$

Eq. (2.2) and Eq. (2.3) relate the change of susceptibilities to the electric field used to fabricate the pattern. Hence the problem of obtaining correlators in

Eq. (2.4) reduces to the problem in determining correlations between UV fields. Below, we proceed to determine the statistical properties of $E_i^{(UV)}\left(\vec{r}\right)$.

Vector components of the UV electric field produced by the diffuser, c.f. Fig. 1, can be found with the help of Rayleigh-Sommerfeld vector diffraction theory [39]:

$$E_x^{(UV)}\left(\vec{r}\right)=-\frac{D+y}{2\pi}\int\int\frac{ik\exp\left[ikR\right]}{R^2}E_{\tilde{x}}^{(UV)}(\tilde{x},\tilde{z})d\tilde{x}d\tilde{z}, \tag{2.5}$$

$$E_y^{(UV)}\left(\vec{r}\right)=\frac{1}{2\pi}\int\int\frac{ik\exp\left[ikR\right]}{R^2}\left(E_{\tilde{x}}^{(UV)}(\tilde{x},\tilde{z})(x-\tilde{x})+E_{\tilde{z}}^{(UV)}(\tilde{x},\tilde{z})(z-\tilde{z})\right)d\tilde{x}d\tilde{z}, \tag{2.6}$$

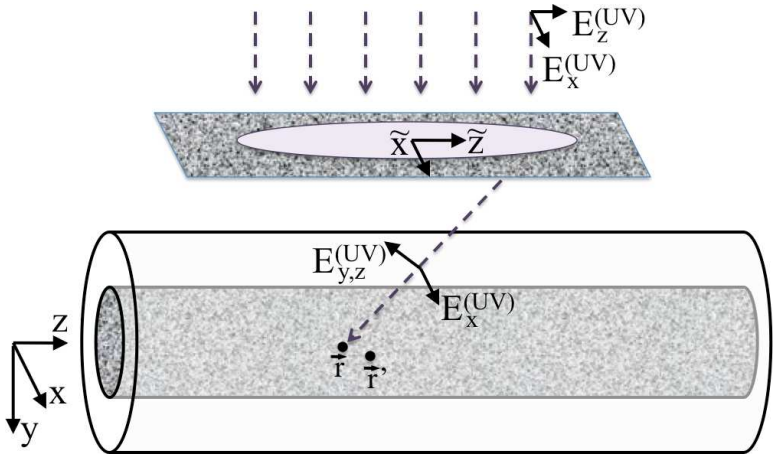

Figure 1: UV irradiation geometry is shown. Expanded unpolarized $\lambda_{UV} = 244nm$ UV light from an Ar laser illuminates an elongated area on the surface of a diffuser. A complex interference pattern is incident onto the core of the Ge-doped photosensitive fiber.

In these equations we adopt the following notations: $(\tilde{x}, \tilde{z})$ are coordinates in the plane of the diffuser; $\vec{r} = (x, y, z)$ are coordinates in the fiber core; $E_{\tilde{x}}^{(UV)}(\tilde{x}, \tilde{z})$ and $E_{\tilde{z}}^{(UV)}(\tilde{x}, \tilde{z})$ are two components of the UV electric fields in the plane of the diffuser; $E_i^{(UV)}(\vec{r})$ are the UV field components in the fiber core; R denotes the distance from $(\tilde{x}, \tilde{z})$ to $\vec{r}$; and $k = 2\pi/\lambda_{UV}$. Expression for $E_z^{(UV)}(\vec{r})$ is analogous to Eq. (2.5).

We assume that the fields originating at the diffuser are δ-correlated Gaussian [55]:

$$\left\langle E_{\tilde{x}}^{(UV)}(\tilde{x}, \tilde{z}) E_{\tilde{x}}^{(UV)*}(\tilde{x}', \tilde{z}') \right\rangle = \left\langle E_{\tilde{z}}^{(UV)}(\tilde{x}, \tilde{z}) E_{\tilde{z}}^{(UV)*}(\tilde{x}', \tilde{z}') \right\rangle$$
$$= (1/2) I_0^{(UV)}(\tilde{x}, \tilde{z}) \kappa \delta(\tilde{x} - \tilde{x}') \delta(\tilde{z} - \tilde{z}'), \qquad (2.7)$$

$$\left\langle E_{\tilde{x}}^{(UV)}(\tilde{x},\tilde{z})E_{\tilde{x}}^{(UV)}(\tilde{x}',\tilde{z}')\right\rangle = \left\langle E_{\tilde{z}}^{(UV)}(\tilde{x},\tilde{z})E_{\tilde{z}}^{(UV)}(\tilde{x}',\tilde{z}')\right\rangle$$
$$= \left\langle E_{\tilde{x}}^{(UV)}(\tilde{x},\tilde{z})E_{\tilde{z}}^{(UV)}(\tilde{x}',\tilde{z}')\right\rangle = 0, \qquad (2.8)$$

where $I_0^{(UV)}(\tilde{x},\tilde{z}) = (\pi L_x L_z)^{-1} \times \exp\left[-\tilde{x}^2/L_x^2 - \tilde{z}^2/L_z^2\right]$ is a Gaussian beam profile, expanded along z-axis, which illuminates the diffuser. Using Eq. (2.5), Eq. (2.6), Eq. (2.7) and Eq. (2.8) we obtain

$$\left\langle E_x^{(UV)}(\vec{r})\, E_x^{(UV)*}(\vec{r}')\right\rangle = \frac{\kappa(D+y)(D+y')}{\lambda_{UV}^2}\int\int \frac{\exp\left[ik(R-R')\right]}{R^2R'^2} I_0^{(UV)}(\tilde{x},\tilde{z})d\tilde{x}d\tilde{z}. \qquad (2.9)$$

The correlation between the other components of the field can be obtained analogously. Because $E_y^{(UV)}(\vec{r})$ depends on the both $E_{\tilde{x}}^{(UV)}(\tilde{x}',\tilde{z}')$ and $E_{\tilde{z}}^{(UV)}(\tilde{x}',\tilde{z}')$ in Eq. (2.6), $\left\langle E_x^{(UV)}(\vec{r})\, E_y^{(UV)*}(\vec{r}')\right\rangle$ and $\left\langle E_y^{(UV)}(\vec{r})\, E_z^{(UV)*}(\vec{r}')\right\rangle$ remain non-zero.

Analytical evaluation of Eq. (2.9) and the corresponding expressions for the other combinations of the field components proves to be challenging under the experimentally relevant conditions, c.f. Ref. [68]. Indeed, the mathematically convenient paraxial approximation is not well justified because the dimensions of the illuminated spot, L_x and L_z, are comparable to the distance to fiber core D. Furthermore, under this approximation $E_y^{(UV)}(\vec{r})$ vanishes entirely and the effect of cross-polarization mode coupling is washed out even though the fiber becomes birefringent because of the strong $E_x^{(UV)}(\vec{r})$.

To circumvent the limitations imposed by the paraxial approximation in Eq. (2.9), we evaluated the integrals numerically. The results shown in Fig. 2 demonstrate that the photo-induced speckle pattern is highly anisotropic. Moreover, correlators $\left\langle E_x^{(UV)}(\vec{r})\, E_y^{(UV)*}(\vec{r}')\right\rangle$ and $\left\langle E_y^{(UV)}(\vec{r})\, E_z^{(UV)*}(\vec{r}')\right\rangle$ field components have $y-z$ and

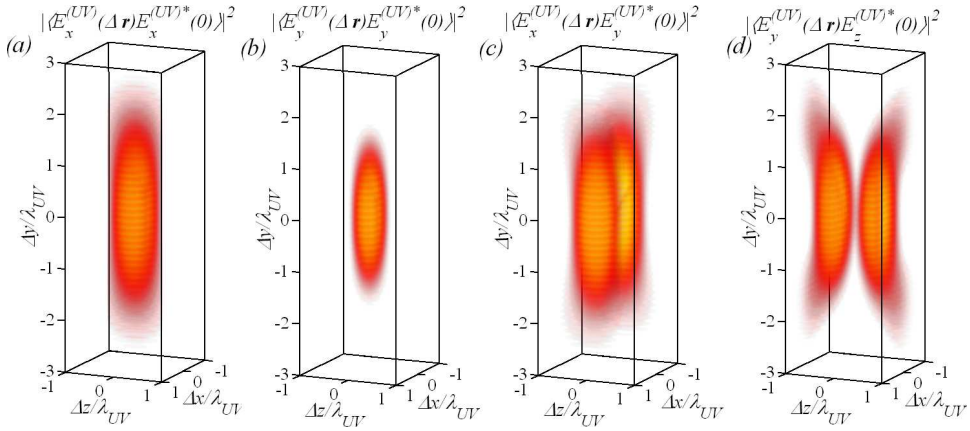

Figure 2: Correlations between field components of the UV light used to fabricate disorder in the core of the photo-sensitive optical fiber. Eq. (2.9) and similar expression for the other field components, originating from Rayleigh-Sommerfeld integrals in Eq. (2.5) and Eq. (2.6), are evaluated numerically under the experimentally relevant conditions – $L_x = 3mm$, $L_z = 5mm$, $D = 5mm$. Not shown are $\left\langle E_x^{(UV)}(\vec{r})\, E_z^{(UV)*}(\vec{r}')\right\rangle$ which vanishes completely and $\left\langle E_z^{(UV)}(\vec{r})\, E_z^{(UV)*}(\vec{r}')\right\rangle$ which is identical to $\left\langle E_x^{(UV)}(\vec{r})\, E_x^{(UV)*}(\vec{r}')\right\rangle$.

$x-y$ nodal planes respectively due to symmetries in the integral in Eq. (2.6) defining y-component of the field. $\left\langle E_x^{(UV)}(\vec{r})\, E_z^{(UV)*}(\vec{r}')\right\rangle$ vanishes completely and correlator $\left\langle E_z^{(UV)}(\vec{r})\, E_z^{(UV)*}(\vec{r}')\right\rangle$ is identical to Eq. (2.9). We note that the effect of refraction of the incident UV light at the air-cladding interface is not accounted for in the derivation of Eq. (2.9), but it is not expected to change our results qualitatively. However we do have to scale the spatial dimensions of the speckles by the refractive index of the fiber core. This can be accomplished by $\lambda_{UV} \to \lambda_{UV}/n_{core}$ substitution in Fig. 2 and Fig. 3.

Scalar theory [68] yields zero $\langle \delta\epsilon_{xy}(\vec{r})\delta\epsilon_{xy}(\vec{r}')\rangle$ and, hence, it does not contain a mechanism to explain cross-polarization coupling by the photo-induced disorder. However, the scalar theory correctly predicts the highly anisotropic structure of correlations in the diagonal components of the dielectric tensor $\langle \delta\epsilon_{ii}(\vec{r})\delta\epsilon_{ii}(\vec{r}')\rangle$. This is a consequence of Eq. (2.2) and Eq. (2.4) (see also Fig. 2(a) and Fig. 2(b)) which is

linked to suppression of the radiative leakage in such a fiber[68]. We expect the same conclusion to hold for theory presented in this work, which properly accounts for the birefringence effects.

The correlators $\left\langle E_i^{(UV)}(\vec{r})\, E_j^{(UV)*}(\vec{r}')\right\rangle$ depend not only on $\Delta\vec{r} \equiv \vec{r} - \vec{r}'$ but also on $\left(\vec{r}+\vec{r}'\right)/2$, due to non-uniform illumination of the diffuser. However, we find that this dependence affects only weakly both magnitude and the shape of the field-field correlators for $-L_z/2 < (z+z')/2 < L_z/2$.

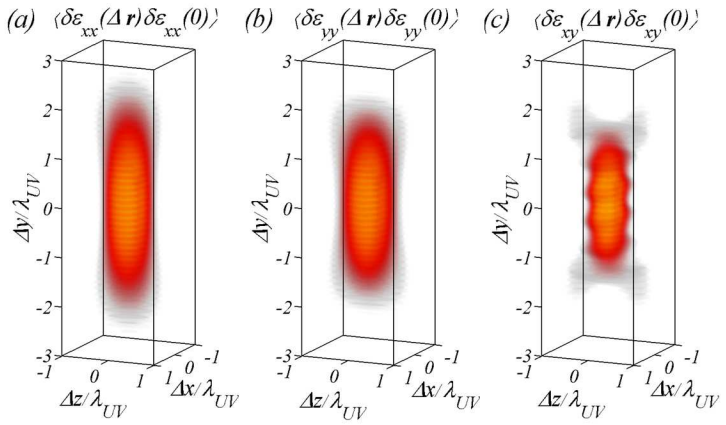

Figure 3: Statistical properties of the spatially fluctuating dielectric tensor are described by correlators $\langle \delta\epsilon_{ij}(\vec{r})\delta\epsilon_{ij}(\vec{r}')\rangle$ in Eqs. (2.12). To evaluate these expression we used the same set of parameters as in Fig. 2. Only the $x-y$ part of the entire tensor relevant to inter-mode coupling are shown.

2.3. Statistical Properties of Disorder. In the next step we obtain the expressions for the photo-induced changes in the dielectric tensor and its fluctuations. Assuming that individual field components represent Gaussian random variables we find the following expression for the change in the spatial average dielectric tensor $\langle\hat{\epsilon}\rangle - n_{core}^2$:

$$\Delta\epsilon_{xx} = \langle\epsilon_{xx}\rangle - n_{core}^2 = C_0\left(4\left\langle\left|E_x^{(UV)}\right|^2\right\rangle + 2\left\langle\left|E_y^{(UV)}\right|^2\right\rangle\right) \tag{2.10}$$

$$\Delta\epsilon_{yy} = \langle\epsilon_{yy}\rangle - n_{core}^2 = C_0\left(2\left\langle\left|E_x^{(UV)}\right|^2\right\rangle + 3\left\langle\left|E_y^{(UV)}\right|^2\right\rangle\right) \tag{2.11}$$

where all off-diagonal elements are equal to zero, $\langle \epsilon_{xx} \rangle = \langle \epsilon_{zz} \rangle$, and we assumed that the diffuser in Fig. 1 is illuminated by an unpolarized beam, i.e. $\left\langle \left| E_x^{(UV)} \right|^2 \right\rangle = \left\langle \left| E_z^{(UV)} \right|^2 \right\rangle$. We immediately observe that the change is anisotropic leading to birefringence. This is an effect well known in fabrication of Bragg gratings [35]. The birefringence along the fiber axis can be suppressed by polarizing the UV light along the axis of the fiber (z-axis), which is in accordance with experiments [38].

Statistical properties of the spatially fluctuating dielectric tensor are described by $\langle \delta\epsilon_{ij}(\vec{r}) \delta\epsilon_{ij}(\vec{r}') \rangle$. Substituting Eq. (2.2) and Eq. (2.3) into Eq. (2.4) we obtain $\langle \delta\epsilon_{ij}(\vec{r}) \delta\epsilon_{ij}(\vec{r}') \rangle / C_0^2$

$$
\begin{aligned}
xx : 10 \left| \left\langle E_x^{(UV)} E_x'^{(UV)*} \right\rangle \right|^2 + \left| \left\langle E_y^{(UV)} E_y'^{(UV)*} \right\rangle \right|^2 + 6 \left| \left\langle E_x^{(UV)} E_y'^{(UV)*} \right\rangle \right|^2 \\
+ 2 \left| \left\langle E_y^{(UV)} E_z'^{(UV)*} \right\rangle \right|^2
\end{aligned}
$$

$$
\begin{aligned}
yy : 2 \left| \left\langle E_x^{(UV)} E_x'^{(UV)*} \right\rangle \right|^2 + 9 \left| \left\langle E_y^{(UV)} E_y'^{(UV)*} \right\rangle \right|^2 + 6 \left| \left\langle E_x^{(UV)} E_y'^{(UV)*} \right\rangle \right|^2 \\
+ 6 \left| \left\langle E_y^{(UV)} E_z'^{(UV)*} \right\rangle \right|^2
\end{aligned}
$$

$$
xy : Re \left[\left\langle E_x^{(UV)} E_x'^{(UV)*} \right\rangle \left\langle E_y^{(UV)} E_y'^{(UV)*} \right\rangle + \left\langle E_x^{(UV)} E_y'^{(UV)*} \right\rangle^2 + c.c. \right], \tag{2.12}
$$

where we use shorthand notations $E_i^{(UV)}(\vec{r}) \to E_i^{(UV)}$ and $E_i^{(UV)}(\vec{r}') \to E_i'^{(UV)}$ and chose to show only a 2×2 section ($x-y$) of the entire tensor, which will be relevant to our further discussion. *c.c.* represents complex conjugate. By substituting the UV field correlators from Sec. 2.2 we obtain the desired result. The spatial correlations in the photo-induced fluctuations of the dielectric tensor are evaluated numerically and shown in Fig. 3. We observe that the general structure of the correlator is similar

to that of $\left|\left\langle E_x^{(UV)} E_x^{\prime(UV)*}\right\rangle\right|^2$, even for $\langle\delta\epsilon_{xy}(\vec{r})\delta\epsilon_{xy}(\vec{r}')\rangle$. The relative magnitudes of different components depend on such factors as the fabrication geometry, c.f. Fig. 1, which allows one to design disordered optical fibers with a desired set of statistical properties.

The natural scale to measure and compare magnitudes of different quantities in Eq. (2.10), Eq. (2.11) and Eq. (2.12) is $\Delta\epsilon_{xx}$. We find that under the experimental conditions $\Delta\epsilon_{yy}/\Delta\epsilon_{xx} \simeq 0.7$, $\langle\delta\epsilon_{xx}^2\rangle/\Delta\epsilon_{xx}^2 \simeq 0.5$, $\left\langle\delta\epsilon_{yy}^2\right\rangle/\Delta\epsilon_{xx}^2 \simeq 0.16$, and $\left\langle\delta\epsilon_{xy}^2\right\rangle/\Delta\epsilon_{xx}^2 \simeq 0.04$. These values will become important when we interpret the results of the experiment further below.

3. HYBRID COUPLED-POWER / COUPLED-MODE THEORY

3.1. Motivation. Even (nominally) single-mode fiber (SMF) supports two propagating modes with orthogonal polarization. Geometric and stress imperfections along the length of the single-mode fiber give rise to randomly varying birefringence [72]. Two perpendicular polarization states of the same mode become coupled with the characteristic length on the order of kilometers. This effect, known as *polarization modal dispersion* (PMD), can be described based on *coupled-mode* equations formalism [73].

In MMF different modes generally propagate with different group delays, an effect known as *inter-modal dispersion*. We note that, although inter-modal dispersion in MMF causes the output intensity profile to change with the propagation distance, it does not lead to the mixing of modes as in PMD in SMF. Meanwhile, various imperfections in the fiber geometry do give rise to mode-coupling described in language of *coupled-power* equations [32, 40]. Increasing concentrations of imperfections to stimulate coupling between the guided modes also inevitably results in coupling to the radiative modes.

In MMF with designed disorder considered in this work *both* cross- and intra-polarization couplings between co-propagating modes occur on the same very short scale of several centimeters. Meanwhile, the radiative leakage occurs at scale one order of magnitude longer. This relationship between different length scales will inform our further analysis.

In choosing the applicable theoretical approach for this problem we were guided by the following considerations. In our system, the coupled-power method cannot provide an adequate description of an evolution of the state of polarization (induced by birefringence) because it does not account for phases of the perpendicular polarization states of the same mode. On the other hand, the couple-mode approach becomes too cumbersome because we consider MMFs supporting a relatively large number (on the order of tens) of modes. This also disallows the continuum approximation in the coupled-power method [69] because this number is not sufficiently large.

3.2. Separation into Deterministic and Stochastic Contributions. In Sec. 2.3 we obtained Eq. (2.10) and Eq. (2.11) for the statistical average dielectric tensor which shows that the fiber becomes (linearly) birefringent. Hence we begin our analysis by expressing the electric field in terms of x- and y- linearly polarized co-propagating modes (orientation of the axes is shown in Fig. 1) in the weakly guiding birefringent step-index fiber with the average dielectric tensor

$$E_i(x,y,z) \approx \sum_{\nu} c_{\nu,i}(z) e^{i(\omega t - \beta_\nu)z} \mathcal{E}_{\nu,i}(x,y). \tag{2.13}$$

Here we adopt mode notations with two subscripts: ν enumerates $N/2$ linearly polarized (LP) modes whereas $i = \{x, y\}$ explicitly denotes the polarization of the mode. $\beta_\nu \equiv (\beta_{\nu,x} + \beta_{\nu,y})/2$ is the propagation constant averaged over two polarization states of ν'th mode. Birefringence results in mode dispersion $\Delta\beta_\nu \equiv$

$(\beta_{\nu,x} - \beta_{\nu,y})$. The transverse field profiles $\mathcal{E}_{\nu,i}(x,y)$ are assumed to be normalized as $\beta_{\nu,i} \int\int [\mathcal{E}_{\nu,i}(x,y)\mathcal{E}_{\nu',i'}(x,y)]\, dxdy = \delta_{\nu\nu'}\delta_{ii'}$, where $\delta_{\nu\nu'}$ and $\delta_{ii'}$ are the Kronecker symbols. In these notations $c_{\nu,i}(z)$ satisfy coupled-mode equations

$$dc_{\nu,i}(z)/dz = (\pm i\Delta\beta_\nu/2 - \alpha/2)\, c_{\nu,i}(z) + \sum_{\nu',i'} \mathcal{K}_{\nu\nu',ii'}(z) c_{\nu',i'}(z) e^{i(\beta_\nu - \beta_{\nu'})z}, \qquad (2.14)$$

where α is the loss coefficient (assumed to be mode independent [29]) and $\mathcal{K}_{\nu\nu',ii'}(z) = (\omega^2/2ic^2) \int\int \mathcal{E}_{\nu,i}(x,y)\delta\varepsilon_{ii'}(x,y,z)\mathcal{E}_{\nu',i'}(x,y)dxdy$ are mode coupling coefficients. The sign of the polarization dispersion term is chosen positive for x and negative for y modes. We note that $x-y$ axes depicted in Fig. 1 constitute principal axes of the statistically averaged dielectric tensor, c.f. Eq. (2.10) and Eq. (2.11).

Next we separate the modal coefficients into a deterministic (ballistic) and random components via

$$c_{\nu,i}(z) = \langle c_{\nu,i}(z) \rangle + \delta c_{\nu,i}(z), \qquad (2.15)$$

where $\langle ... \rangle$ denotes disorder average. By definition $\langle \delta c_{\nu,i}(z) \rangle \equiv 0$. Below we describe the deterministic component with coupled-mode (amplitude) equations whereas the random contribution will be treated within the coupled-power approach. In doing so, we explicitly account for polarization rotation only in the transition regime (via coupled-mode equation for the amplitudes) of sufficiently short samples when the ballistic signal has not yet had a chance to reach the equilibrium mode distribution. As the energy is removed from the ballistic signal and transfered into randomly phased component, described by $\delta c_{\nu,i}(z)$, the effects of inter-mode scattering and polarization dispersion compete. Therefore, the coupled-power description of $\delta c_{\nu,i}(z)$ is justified because, as it will be evident from the experimental analysis in Sec. 4, both processes occur on the same characteristic length scale *and* because the

inter-mode scattering also involves *cross-polarization coupling* on the similar scale, c.f. Eqs. (2.12).

3.3. Coupled-Mode Description of Mode Amplitudes. Obtaining the evolution equations for $\langle c_{\nu,i}(z)\rangle$ from Eq. (2.15) involves the task of computing values for $\langle \mathcal{K}_{\nu\nu',ii'}(z)c_{\nu',i'}(z)\rangle$. The latter can be accomplished by employing approach used in an analysis of dynamical systems. First, we formally integrate Eq. (2.15) to obtain $c_{\nu',i'}(z)$ on the left hand side of the equation. Then we multiply both sides by $\mathcal{K}_{\eta\nu,ji}(z)$ and perform a statistical average. Assuming that $\delta\epsilon_{ij}(x,y,z)$ is a random delta-correlated Gaussian process, enables us to compute the average. This assumption is justified because there is a large disparity in correlation scales between $c_{\nu',i'}(z)$ and $\delta\epsilon_{ij}(x,y,z)$ – centimeters and λ_{UV} respectively, c.f. Sec. 2.2. We obtain

$$d\left\langle c_{\nu,i}(z)\right\rangle /dz = \left(\pm i\Delta\beta_{\nu}/2 - \alpha/2 - h_{\nu,i}/2\right)\left\langle c_{\nu,i}(z)\right\rangle , \tag{2.16}$$

with coupling coefficients are defined by

$$h_{\nu,i} = \sum_{\nu'',i''} h_{\nu\nu'',ii''} \tag{2.17}$$

$$h_{\nu\nu'',ii''} = \left(\omega^4/4c^4\right)\left\langle \delta\epsilon_{ii''}\delta\epsilon_{i''i}\right\rangle V_{ii''i''i}\int\int \mathcal{E}^2_{\nu,i}(x,y)\mathcal{E}^2_{\nu'',i''}(x,y)dxdy, \tag{2.18}$$

where we approximated $\left\langle \delta\epsilon_{ii''}\left(\vec{r}\right)\delta\epsilon_{i''i}\left(\vec{r}''\right)\right\rangle \simeq \left\langle \delta\epsilon_{ii''}\delta\epsilon_{i''i}\right\rangle V_{ii''i''i}\delta\left(\vec{r}-\vec{r}''\right)$. $V_{ii''i''i}$ is the correlation volume of the UV speckle pattern of the fabricated disorder, c.f. Sec. 2.2 and Ref. [68]. In arriving at Eq. (2.16) we neglected the terms involving $\langle c_{\nu',i'}(z)\rangle$ cross channel scattering, $\nu \neq \nu'$, $i' \neq i$, on the right hand side. This is justified because: (a) for co-polarized modes coupling term involves factor $\int\int \mathcal{E}_{\nu,i}(x,y)\mathcal{E}^2_{\nu'',i''}(x,y)\mathcal{E}_{\nu',i}(x,y)dxdy$ which is small for $\nu \neq \nu'$ due to orthogonality

of $\mathcal{E}_{\nu,i}(x,y)$; (b) for cross-polarized modes the factor $\langle \delta\epsilon_{ii''}\delta\epsilon_{i''i'}\rangle$ is small ($i \neq i'$), c.f. Sec. 2.3.

We conclude this section by writing the solution of the derived Eq. (2.16)

$$\langle c_{\nu,i}(z)\rangle \simeq c_{\nu,i}(0)\exp\left[(\pm i\Delta\beta_\nu/2 - \alpha/2 - h_{\nu,i}/2)\, z\right] \tag{2.19}$$

where $c_{\nu,i}(0)$ denote the modal amplitudes upon injection into the fiber at $z = 0$. The solution above describes the evolution of the state of polarization of ν'th mode and its exponential attenuation due to loss (α term) and decoherence ($h_{\nu,i}$ term). This latter process transfers power from the ballistic to random component, which we treat next.

3.4. Coupled-Power Equations for Random Component. Derivation for the coupled power equations [68] satisfied by $P^{(\delta)}_{\nu,i} \equiv \left\langle |\delta c_{\nu,i}|^2 \right\rangle$ leads to a new source term $h_{\nu,i}P^{(b)}_{\nu,i}(z) \equiv h_{\nu,i}\left|\langle c_{\nu,i}(z)\rangle\right|^2$ in the otherwise cannonical coupled power equation [40]:

$$dP^{(\delta)}_{\nu,i}/dz = h_{\nu,i}P^{(b)}_{\nu,i} - \alpha P^{(\delta)}_{\nu,i} + \sum_{\nu',i'} h_{\nu\nu',ii'}\left(P^{(\delta)}_{\nu',i'} - P^{(\delta)}_{\nu,i}\right). \tag{2.20}$$

The source term represents in-flux from the ballistic component described by Eq. (2.16). The above equation should be supplemented with the initial conditions $P^{(\delta)}_{\nu,i}(0) = 0$.

The approximate solution of Eq. (2.20) can be obtained at both small and large values of z. For modes with non-zero (ballistic) source terms we find $P^{(\delta)}_{\nu,i}(z) \approx h_{\nu,i}\left|c_{\nu,i}(0)\right|^2 \times z$ and $P^{(\delta)}_{\nu,i}(z) \approx \left[\sum_{\nu',i'} h_{\nu\nu',ii'}h_{\nu',i'}\left|c_{\nu',i'}(0)\right|^2\right] \times z^2$ for the rest. This solution is valid for $z < \min[h_{\nu,i}]$. For $z \gg \sigma_2$ when the source terms become negligible, the power becomes equipartitioned among all N modes $P^{(\delta)}_{\nu,i}(z) \approx (1/N)\exp[-\alpha z]$. Here $\sigma_2 \sim h_{\nu\nu',ii'}$ denotes the second smallest eigenvalue of the secular equation $\det\left[h_{\nu\nu',ii'} + (\sigma - h_{\nu,i})\,\delta_{\nu\nu'}\delta_{ii'}\right] = 0$ [40, 68].

To obtain solution for arbitrary z we use the forth order Runge-Kutta method to solve Eqs. (2.20) numerically under experimentally relevant conditions; $\alpha = 0$ is assumed for clarity. At $z = 0$ the only non-zero terms are $c_{\nu,x}(0) = (2/N)^{1/2}$. Figure 4(a) depicts $P^{(\delta)}_{\nu,x}(z)$ and $P^{(\delta)}_{\nu,y}(z)$ as blue and gold lines respectively. $P^{(\delta)}_{\nu,x}(z)$ are peaked at small z before equilibration is reached among the modes of both polarizations. The dashed line depicts the $1/N$ level. We observe that efficient cross-polarization coupling due to induced birefringence makes intra- and inter-polarization equilibration occur at similar lengths scales, i.e. $\sigma_2^{-1} \sim 2\sigma_3^{-1}$ which is explicitly confirmed numerically. The inset in Fig. 4(a) depicts $\sum_\nu P^{(\delta)}_{\nu,i}(z)$ demonstrating an equilibration at 1/2 level shown as a black dashed line. Also depicted are the ballistic component $\sum_\nu P^{(b)}_{\nu,x}(z)$, dashed line, and the total power in x polarization $\sum_\nu P^{(b)}_{\nu,x}(z) + \sum_\nu P^{(\delta)}_{\nu,x}(z)$, dotted line.

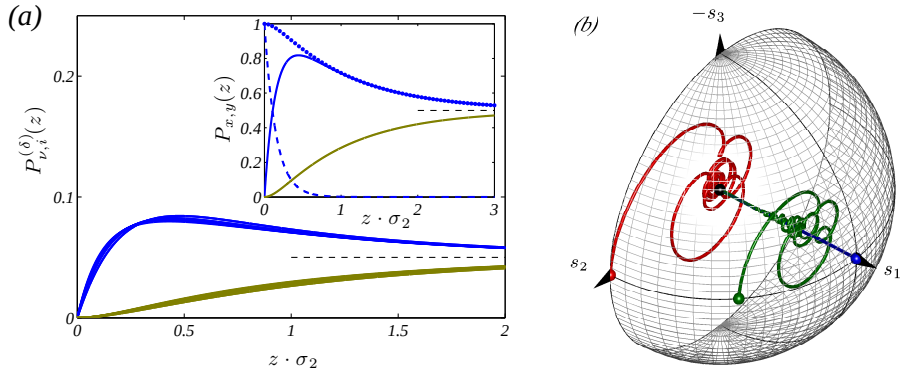

Figure 4: (a) Runge-Kutta numerical solution of Eqs. (2.20) with $\alpha = 0$. Only x-polarized LP modes are exited: $c_{\nu,x}(0) = (2/N)^{1/2}$. The power becomes equally distributed among the modes of both polarizations (x – blue, y – gold) before equilibrating at $1/N$ level shown as a dashed line. $\sum_\nu P^{(\delta)}_{\nu,i}(z)$ converging at 1/2 are shown in the inset. The ballistic component $\sum_\nu P^{(b)}_{\nu,x}(z)$ and the total power in the x polarization $\sum_\nu P^{(b)}_{\nu,x}(z) + \sum_\nu P^{(\delta)}_{\nu,x}(z)$ are depicted with dashed and dotted lines respectively. (b) Evolution along the fiber length of elements of the Stokes vector $\vec{s}(z)$. The Poincaré sphere plot describes the transition from the linearly polarized light with the degree of polarization $\mathcal{P} \equiv |\vec{s}| = 1$ at $z = 0$ to unpolarized light with $\mathcal{P} = 0$ in the limit $z \to \infty$. Blue, green and red lines correspond to the light linearly polarized at $\phi = 0$, $\pi/8$, and $\pi/4$ with respect to the x primary axis of the average dielectric tensor respectively.

3.5. De-Polarization and Stokes Parameters. The direct consequence of the cross-polarization mode coupling caused by the induced birefringence, c.f. Eq. (2.12), is a de-polarization of the initial excitation. This process is conveniently described by Stokes parameters [74]. Separation of the modal amplitudes into the deterministic (ballistic) and random contributions, c.f. Eq. (2.15), enables us to obtain the following expressions:

$$\begin{aligned}
S_0 &= \textstyle\sum_{\nu=1}^{N/2} \left(P_{\nu,x}^{(b)} + P_{\nu,x}^{(\delta)} - P_{\nu,y}^{(b)} - P_{\nu,y}^{(\delta)} \right); \\
S_1 &= \textstyle\sum_{\nu=1}^{N/2} \left(P_{\nu,x}^{(b)} + P_{\nu,x}^{(\delta)} - P_{\nu,y}^{(b)} - P_{\nu,y}^{(\delta)} \right); \\
S_2 &= \textstyle\sum_{\nu=1}^{N/2} \left(\langle c_{\nu,x} \rangle \left\langle c_{\nu,y}^* \right\rangle + \left\langle c_{\nu,x}^* \right\rangle \langle c_{\nu,y} \rangle \right); \\
S_3 &= i \textstyle\sum_{\nu=1}^{N/2} \left(\langle c_{\nu,x} \rangle \left\langle c_{\nu,y}^* \right\rangle - \left\langle c_{\nu,x}^* \right\rangle \langle c_{\nu,y} \rangle \right).
\end{aligned} \tag{2.21}$$

Three-component Stokes vector is defined as $s_{1-3} = S_{1-3}/S_0$. In these notations the fully polarized light, regardless of its state of polarization, corresponds to the Stokes vector at the surface of the Poincaré sphere $|\vec{s}| = 1$. In contrast, a completely unpolarized light has the state of polarization $\mathcal{P} \equiv |\vec{s}| = 0$.

Figure (4) depicts the evolution of the Stokes vector along the length of the fiber. Blue, green and red lines correspond to the initial linear polarizations at the angles $\phi = 0, \pi/8, \pi/4$ with respect to the principal axis of the fiber: $c_{\nu,x} = (2/N)^{1/2} \cos(\phi)$, $c_{\nu,y} = (2/N)^{1/2} \sin(\phi)$ is assumed. In each case, we observe a relaxation of the state of polarization from $\mathcal{P} = 1$ at $z = 0$ to $\mathcal{P} = 0$ at $z \gg \sigma_2^{-1}$. This concludes our demonstration of complete mixing on the same short length scale σ_2^{-1} of the both co- and cross-polarized modes in the artificially disordered fiber.

4. EXPERIMENTAL CORROBORATION

4.1. Experimental Setup. In this experiment we employed a step-index silica fiber doped by Ge (PS1250/1500 of Fibercore). The main parameters of the fiber are a core diameter of $7.66\mu m$, cladding diameter of $125\mu m$, and numerical aperture (NA) of 0.13, with the refractive indices of the core and the cladding being 1.463 and 1.457, respectively. Three samples of fiber (about $20cm$) included the disordered part of 2, 4 and $12cm$ respectively. Fabrication and characterization of the volume disorder is described in details in Ref. [68].

At the input of the optical fiber the polarized light goes through a half wave-plate and a linear polarizer oriented along axis x', which makes angle ϕ with respect to the principal axis of the fiber x. The output light was detected separately for both polarizations: a) after passing through a polarizer of the same orientation as at the input ($x'x'$ - polarization), or b) perpendicularly polarized ($x'y'$ - polarization). We analyzed the output light of each polarization independently. Measurement was repeated 10 times for different random bending of the fiber. The bending of the fiber was sufficient to change the disorder but not sufficient to introduce appreciable additional birefringence. Both polarizers were rotated synchronously by 10° (i.e. ϕ was incrementally increased) and measurements were repeated.

At the probe laser light wavelength $\lambda = 543nm$ used in measurements, the number of guided LP modes (counting both polarizations) is $N = 20$. The average integrated intensity of outgoing light for two perpendicular orientations of the polarizer are presented in Fig. 5 for rotations in the interval $0° - 90°$.

4.2. Comparison of Theory and Polarization-Resolved Measurement. After obtaining the solutions for $\langle c_{\nu,i}(z)\rangle$ and $P^{(\delta)}_{\nu,i}(z)$ describing the evolution of the ballistic and stochastic components in Eq. (2.15) in the principal axes coordinate

system $x-y$, we perform the coordinate transformation to the axes $x'-y'$ rotated by angle ϕ. We obtain

$$P\begin{bmatrix} x' \\ y' \end{bmatrix} = P_x \begin{bmatrix} \cos(\phi)^2 \\ \sin(\phi)^2 \end{bmatrix} + P_y \begin{bmatrix} \sin(\phi)^2 \\ \cos(\phi)^2 \end{bmatrix} \pm 2\sin(\phi)\cos(\phi)\Re\left[\sum_\nu \langle c_{\nu,x}\rangle \langle c^*_{\nu,y}\rangle\right], \tag{2.22}$$

where $P_i \equiv |\langle c_{\nu,i}\rangle|^2 + P^{(\delta)}_{\nu,i}$ and $\Re[\ldots]$ denotes the real part.

Eq. (2.22) can be evaluated numerically as in Sec. 3.4. However, it is illuminating to find a closed-form analytical expression describing the evolution of power in each polarization $P_{i'}$. This task can be accomplished with an assumption that the asymptotic expression for $P_i(z) = [(P_i(0)-1/2)\exp(-\sigma_2 z)+1/2]\exp(-\alpha z)$ is valid for the entire range of $0<z<\infty$. The inset in Fig. 4 shows the adequacy of such an approximation. We arrive at our final result

$$P\begin{bmatrix} x' \\ y' \end{bmatrix}(z) = e^{-\alpha z}\left\{\left(P_x(0)\begin{bmatrix} \cos(\phi)^2 \\ \sin(\phi)^2 \end{bmatrix} + P_y(0)\begin{bmatrix} \sin(\phi)^2 \\ \cos(\phi)^2 \end{bmatrix} - \frac{1}{2}\right)e^{-\sigma_2 z} + \frac{1}{2}\right.$$
$$\left. \pm 2\sin(\phi)\cos(\phi)\frac{2}{N}\sum_\nu P^{1/2}_{\nu,x}(0)P^{1/2}_{\nu,y}(0)\exp\left(-\frac{h_{\nu,x}+h_{\nu,y}}{2}z\right)\cos\left(\Delta\beta_\nu z\right)\right\} \tag{2.23}$$

where, as previously, we take $P_x(0)+P_y(0)=1$. The above expression describes the following effects: (i) attenuation due to radiative losses – α term; (ii) assymptotic equal distribution of power over all N co-propogating modes of the fiber – σ_2 term; (iii) de-polariation of the incindent light – $h_{\nu,i}$ term; (iv) change of the polarization state is the decaying ballistic signal – $\Delta\beta_\nu$ term. Furthermore, the expression above conserves power at every z. Figure 5 demonstrates that Eq. (2.23) describes the experiment well: it captures both the polarization and length dependences of the transmitted signal.

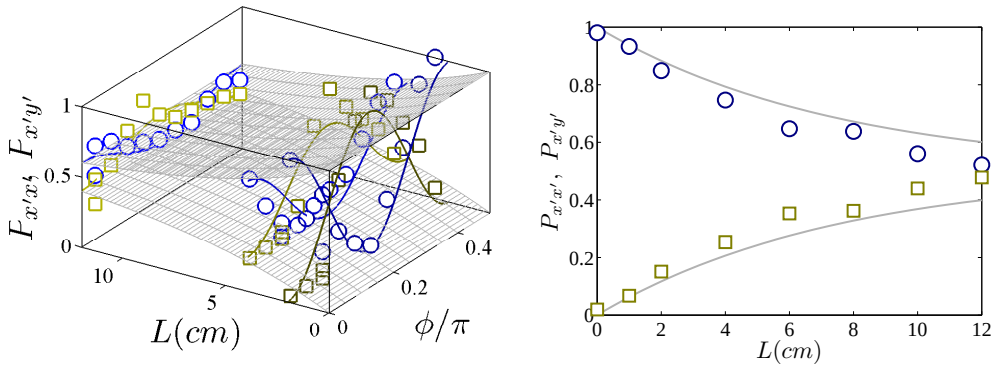

Figure 5: (a) Experimental data in $L = 2, 4$ and $12cm$ samples for the ensemble-averaged transmission for $x'x'$ (circles) and $x'y'$ (squares) polarization channels as the function of the angle ϕ between x' and the principal axis x. In all cases the incident light is polarized along x' axis. For clarity, the data is normalized as $P_{x'x'}(z) \to P_{x'x'}(z)/\int (P_{x'x'}(z) + P_{x'y'}(z))\, d\phi$ and similarly for $P_{x'y'}(z)$ to eliminate the effect of attenuation $\times \exp(-\alpha z)$. Solid lines show the theoretical fit with Eq. 2.23 by combining the $\sum_\nu$ term into a single fitting parameter. Two converging surface envelopes $1/2 \pm \exp(-\sigma_2 z)/2$ are shown a guide for an eye demostrating almost complete mode mixing at $L = 12cm$. (b) Normalized by $P_x(z) + P_y(z)$ to eliminate the $\exp(-\alpha z)$ factor, $P_x(z), P_y(z)$ show convergence toward $1/2$. To acheive alighnment with the principal axes of fiber, the experimental data (symbols) was obtained in-situ during fabrication of the additional segments of disordered fiber. Solid lines obtained for $\phi = 0$ from the fit in (a) show somewhat slower decay, that is attributed to unintentional twisting in process of generating ensemble realizations by bending of the fiber.

5. CONCLUSIONS

In this work we obtained two main results. First, beginning with a microscopical model of photo-sensitivity in a germano-silicate glasses, we analytically derived formulae describing the spatial correlations between the components of the dielectric tensor, c.f. Sec. 2.3. We made the connection between the statistical properties, including the polarization statistics, of the incident UV light and those of the artificial disorder inscribed in the core of the fiber. Importantly, as it has been shown by Korotkova in Ref. [75], the statistics of (the UV) light changes when the light propagates in a free space. This suggests that the spatial properties of the UV light, and hence of the artificial disorder, can be manipulated by altering the illuminations geometry during the disorder writing process.

The second result concerns the description of the light propagation in the fiber with the artificially correlated disorder. Our previous study based on coupled power theory [68] could not explain strong mixing of cross-polarized co-propagating modes observed experimentally. We suggested that an induced birefringence might be the cause. This work shows that the actual answer is more complicated. On one hand, the existence of the linear birefringence *on average*, c.f. Eq. (2.10) and Eq. (2.11), causes only a periodic evolution of the two polarization states of each mode in the fiber. By itself this effect does not lead to equilibration of power among all modes in two polarization channels. Instead, the coupling is the result of the non-zero correlations between the off-diagonal components of the dielectric tensor, c.f. Eq. (2.12), which in turn are caused by the non-trivial correlations between $x-$ and $y-$ components of the UV writing beam, c.f. Fig. 2. Unlike intra-polarization coupling, the magnitude of the cross-polarization coupling is directly related to existence of the longitudinal component of the UV field used in fabrication of disorder. Thus, our choice of the near-field illumination (small reparation between diffuser and fiber in Fig. 1)

is critical. Our theory predicts significantly weaker coupling between orthogonally-polarized modes in the paraxial regime when the only remaining coupling due to bending-stresses may become dominant.

Modeling light propagation in the disordered birefringent fiber poses a challenge for a coupled-power description. In fact, it becomes inadequate because coherent process of evolution of polarization cannot be captured. To overcome this limitation, in this work we developed a hybrid theory which treats the deterministic (ballistic) part of the light via coupled-amplitude equations, whereas the randomly-phased component is treated with a coupled-power equations, c.f. Sec. 3. Neglecting the polarization change in the random component is justified in our artificially disordered fiber because the process of scattering occurs on a very short length scale on the order of $1cm$.

Comparison with experiment in Sec. 4 suggests that very short $\sim 10cm$ segments of the fabricated multi-mode fibers with designed disorder can be used as mode-scrambler / descrambler mixing efficiently all modes with both states of polarization. Furthermore, we previously estimated and confirmed experimentally that the mixing can be accomplished without significant radiative losses, $3.6dB$ in Ref. [68]. This makes our fibers with custom-made disorder suitable for such applications as e.g. hardware encryption and power-management in high-power fiber laser systems. The complete mode mixing is also required to achieve the maximum channel capacity in MIMO transmission in the multi-mode optical fibers.

6. ACKNOWLEDGMENTS

The work at Missouri S&T was supported by the University of Missouri Research Board and by the National Science Foundation Grant No. DMR-0704981.

NPP and EIC would like to acknowledge a support by CONACYT (México), under grant UCM-42127.

III. INVESTIGATION OF MODE COUPLING IN OPTICAL FIBER WITH CONTROLLED VOLUME DISORDER

[1]*N. P. Puente,* [2]*E. I. Chaikina,* [3]*S. Herath and* [3]*A. Yamilov*

[1]*Facultad Ingenieria-Ensenada, Universidad Autonoma de Baja California, Ensenada, B.C., 22860, México*

[2]*División de Física Aplicada, Centro de Investigación Científica y de Educación Superior de Ensenada,B.C., 22860, Ensenada, México*

[3]*Department of Physics, Missouri University of Science & Technology, Rolla, MO 65409*

ABSTRACT*

This paper presents results of experimental and theoretical studies of light transmission through optical fibers with disorder generated in its germanium-doped core via UV radiation transmitted through a diffuser. The experimental results on transmission of the radiation of 543 nm wavelength demonstrate the presence of the disorder in the core of the optical fiber beyond certain characteristic length, the transmitted power is observed to be distributed over all modes of the fiber. A theoretical model based on coupled-power theory is developed. An analytical expression

*Proceeding of SPIE Vol 7839, 78391O-1 , (2010).

for the mixing length is obtained and agrees well with the experiment. For long sections of disordered fiber, the experimentally measured distribution of the near-field intensity at the output surface of the fiber is well described by the Rayleigh negative exponential function. This suggests a statistically uniform distribution of the transmitted power over all modes, that agrees with the prediction of the theoretical model. The reported technique provides an easy way to fabricate different configurations of the controlled disorder in optical fibers suitable for such applications as random fiber lasers. Keyword: multiple scattering; fiber optics; coupling theory.

1. INTRODUCTION

During recent years, there has been a considerable interest in optical disordered media. This is largely due to the important benefits observed when a disorder is induced into a rmundane systems. Random laser[76], where laser action is ensured by a coherent feedback in disordered structures, such as powder or porous crystals, is a striking example. In the paper[21] the advantages of the disordered systems in wireless communications of high information capacity have been shown. It has also been reported[42] that the disorder induced in nonlinear crystals can greatly improve efficiency of operation of the nonlinear optical devices. It appears that disordered media open numerous possibilities for applications in sensors, nanophotonics and, more generally, in various system of light transmission.

In this report we present experiments on fabrication of random variations of the refractive index throughout the core of Ge-doped optical fiber, whose parameters can be controlled in our experimental setup. The characteristics of the created disorder are evaluated from an analysis of the intensity distribution of the near-fields at the output of the fiber and by the analysis of the size dependence of the total intensity of the transmitted light. The experimental results are compared and an agreement is found with the predictions of the coupled-power theory which is adapted to the particular type of volume disorder considered in this work.

1.1. Fabrication of the Disorder. The experimental setup utilized for the fabrication of the disorder in optical fibers is schematically depicted in Fig. 1. In our experiments we employed the step-index optical fiber (PS1250/1500 of Fiber core) sensitized by Ge. The main parameters of the fiber are: the core diameter is 7.66 microns, the cladding diameter is 125 microns, NA = 0.13 with the refractive index of the core and the cladding 1.463 and 1.457, respectively. The cutoff wavelength of

the fiber with these parameters was about 1200 nm. The volume disorder was introduced in the Ge-doped fiber core by exposing it to the UV light from an intracavity frequency doubled Argon-ion laser (244nm) which passed through a cylindrical lens and a diffuser creating, in this way, a speckle pattern in the plane parallel to the fiber axis. The light beam generated by the UV laser was initially expanded by a cylindrical lens with the focal length 12 cm in order to form the necessary spot width on the diffuser plane. The beam transmitted through the diffuser was used for exposing the photo-sensitive fiber. Speckle, as the strongly fluctuating, grainy intensity pattern resulting from the interference of randomly scattered coherent waves, resulted in fluctuations of the illuminating UV intensity in the fiber core. The average speckle spot size is defined as[77] $r = \lambda * d/\pi * w$ where is the distance between the diffuser and Variations of the in the range 2-8 mm and of in the range of 8-10 mm allowed us to obtain the average speckle size between 200 and 600 nm.

The length of each segment with the fabricated disordered length was 1-2 cm. Experimental geometry allowed us to record the segments with greater lengths (50 mm). In order to achieve the disorder with similar statistical parameters in each segment, the exposure time was used the same for all segments, and namely, about 10 minutes at mean power of the UV laser about 60 mW. We observed experimentally that after this exposure the intensity distribution of the output probe light at the fiber output didn't change. Every next segment with random distributed of the refractive index was recorded directly after the preceding one. The total lengths of the fabricated disordered part were of 2, 4, 6, 8, 10 and 15 cm. It is noteworthy to mention that fabrications of the longer samples was not necessary because, after passing 8 cm of the disordered fiber, the transmission saturates and practically stops changing with an increase of the disordered part of the fiber.

After forming the bulk disordered segment we launched the probe beam of the He-Ne laser operated at nm into the fiber, and detected the image of the output

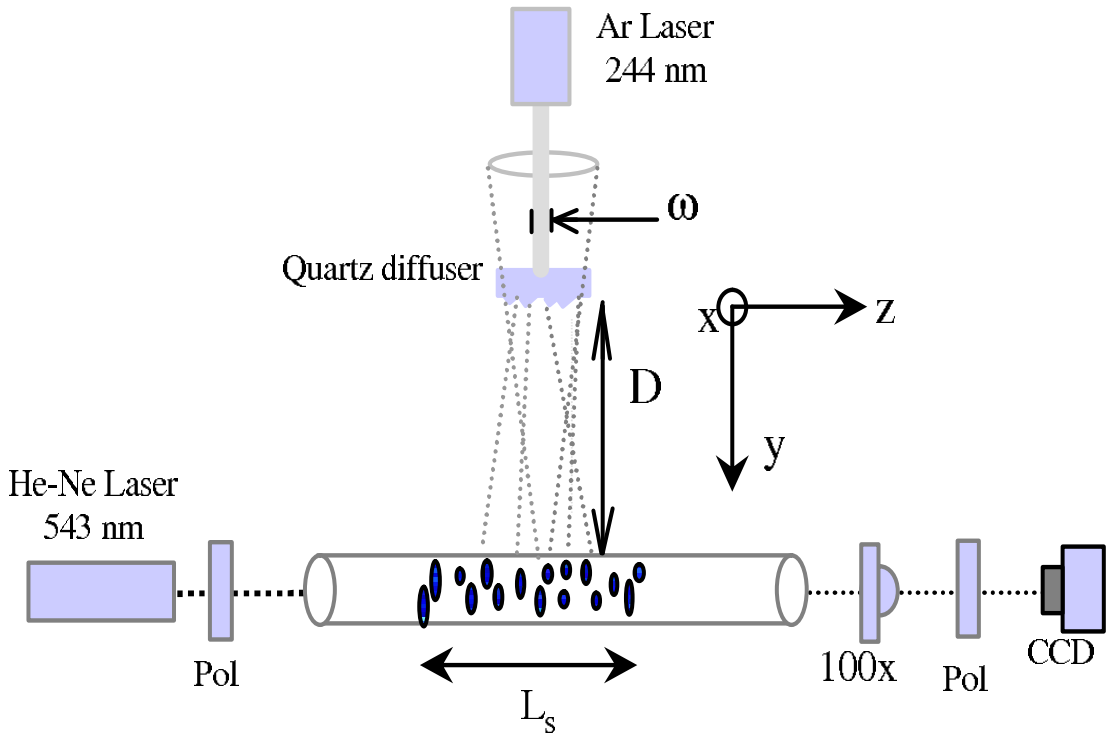

Figure 1: The experimental setup.

intensity distribution by a charge-coupled device (CCD camera, ST-402ME SBIG). The selected wavelength 543 nm of the probe beam ensured a low mode-number propagation regime and corresponded to the sensitivity range of the CCD camera quite well. The light emerging from the fiber passed through the microscope objective x100 which imaged the output fiber plane on the CCD camera. In front of the CCD camera there was a polarizer utilized for characterization of the transmitted light.

2. EXPERIMENTAL RESULTS

The resulting V parameter of the utilized fibers was 5.8171 at the probe wavelength and the expected number of the guided linearly polarized LP_lm modes is 20. By varying the angle of the probe beam incidence, different combinations of modes

were excited and the corresponding near-field transmitted intensity was recorded. It appears that these measurements can be made quite reliably. Indeed, (i) the light polarization was preserved in the fiber without disorder; (ii) the ambient temperature fluctuations did not change significantly the parameters of the fiber samples during measurements. At the input of the optical fiber, the polarized light goes through a half wave-plate and a linear polarizer. The output light was detected separately for both polarizations: a) after passing through a polarizer of the same orientation as at the input (pp - polarization) or b) perpendicularly polarized (ps - polarization). We analyzed the the output light of each polarization independently. The polarization extinction ratio of the laser source and the fiber output was measured in the linear transmission regime respectively.

The examples of the intensity distribution of the light emerging from the fiber obtained for different realizations and for different angles of the incident beam with the disordered segment of the fiber of 1 cm (a) and 2 cm (b) long are presented in Fig.2. Left column corresponds to pp-polarization measurements , right columns represents ps polarization measurements. Different realization was obtained by slightly bending of the disordered part of the fiber.

In Fig.3 the ensemble averaged intensities of the output light measured experimentally as function of the length of the disordered parts of the fiber is presented. The averaging was performed over 10 realizations. One can see that with increasing of angle of incidence, that increases the weightr coefficients for the higher order modes, the characteristic length of the mode coupling goes down.

3. COUPLED-MODE THEORY IN FIBERS WITH BULK RANDOM PERTURBATIONS OF REFRACTIVE INDEX

The data presented in Figs.2,3 suggests that the random fluctuations of refractive index imprinted in the core of a photo-sensitive fiber result in mixing among

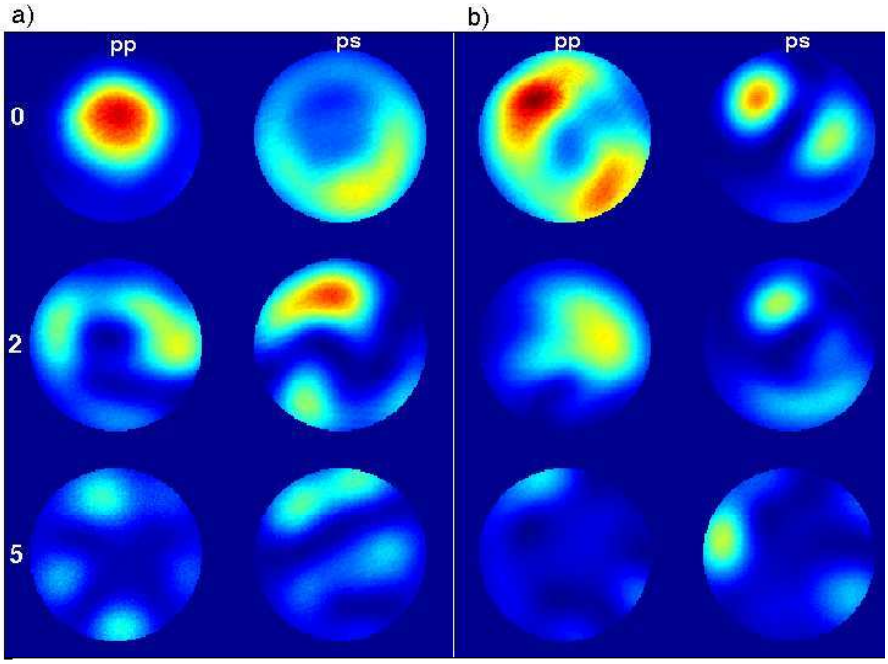

Figure 2: The output intensity distribution observed in some realizations with the disordered part of the fiber 1 cm (a) and 2 cm (b) length; left column in each figure presents pp polarized distribution, and right column presents the ps polarized one. The angles of incidence are 0°, 2° and 5° from the top to the bottom images.

different propagating modes. To describe this process and to obtain the characteristic (mixing) length of the disordered segment of fiber, we employ the coupled-power method developed by Marcuse[40]. However, because the disorder induced by the UV speckle pattern does not allow a factorization of the refractive index modulations into the functions of the transverse and longitudinal coordinates $\delta n(x, y, z) = \delta n(x, y) times f(z)$, the original derivation is not applicable. We demonstrate that the coupled-power theory can still be developed due to the factorization of the disorder's second order correlator

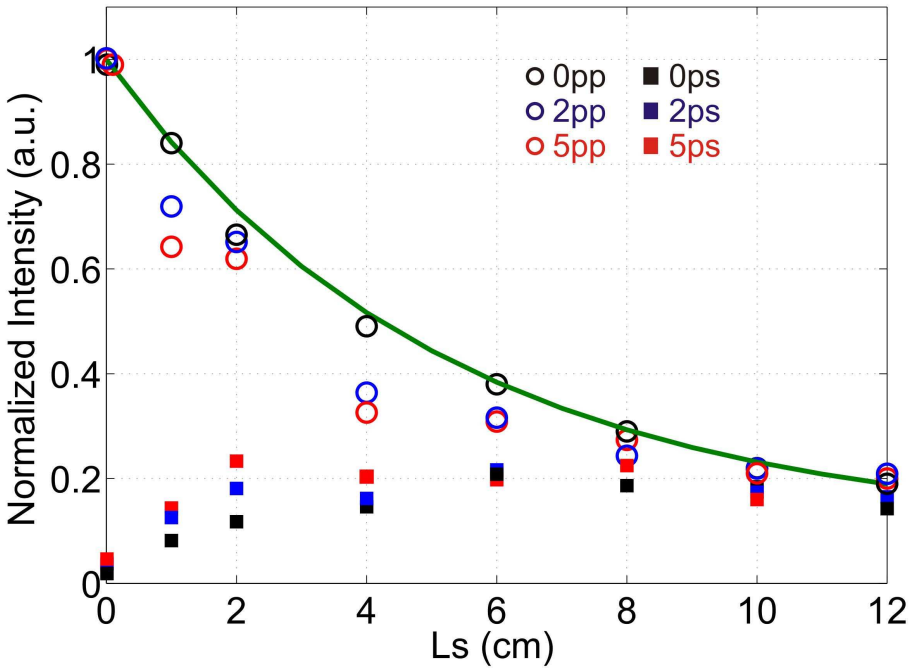

Figure 3: Experimentally observed total transmission as a function of the length of the disordered part of the fiber. The black symbol correspond to 0° of the angle of incidence, the blue symbols to 2°, and the black ones to 5°.

$$\langle \delta\varepsilon(\mathbf{r})\delta\varepsilon(\mathbf{r}')\rangle \approx \langle \delta\varepsilon^2\rangle \exp\left[-\left(\frac{x-x'}{S_x}\right)^2\right] \frac{1}{\left[1+\left(\frac{y-y'}{S_y^2}\right)^2\right]^{1/2}} \exp\left[-\left(\frac{z-z'}{S_z}\right)^2\right]. \tag{3.1}$$

where $\delta\varepsilon(\mathbf{r})$ is the fluctuation of the dielectric function due to presence of disorder and $S_{x,y,z}$ correspond to the speckle dimensions. The derived equation

$$\frac{dP_\mu}{dz} = \sum_\nu \left[h_{\mu\nu}P_\nu - h_{\nu\mu}P_\mu\right] \tag{3.2}$$

describes the evolution of the disorder-averaged power in each mode P_μ . The obtained expression for the coupling coefficients (not shown here due to space considerations) allows one to compute a characteristic length after which modes become perfectly mixed. Its expression can be simplified to obtain the following analytical result

$$\ell^{(xx)-1} \sim \frac{\Delta n}{2n_{core}} \frac{\pi\omega^2 S_x S_y S_z}{c^2 a^2} \tag{3.3}$$

where a is the core radius. Substituting the experimental parameters of the system we find $l_{mixing} \approx 5cm$. The agreement with the experimental data shown in Fig.3 is good, given the fact that the exact value of Δn is not directly accessible, we estimated it to be of the order of $10^{-}4$.

One known prediction of a coupled mode theory is that the power is equally distributed over all modes of the fiber[40]. The fact that the intensity transmitted through the long sections of the disordered fiber reaches a saturation (within experimental precision) beyond L=15cm agrees well with the theoretical predictions. It also suggests that the coupling to the radiative modes and other loss mechanism do not play a significant role in transmission. The conclusion that a perfect mixing (in statistical sense) occurs in our experimental system can also be tested through measurements of the statistical distribution of the polarization-resolved near-field intensity. Indeed, a random sum of different modes of the fiber is expected[55] to result in the Rayleigh negative exponential distribution. This predict based on the above theory is fully borne out experimentally.

4. ACKNOWLEDGMENTS

NPP and EIC would like to acknowledge support from by CONACYT (Mxico), under grant No.UCM-42127. The work at Missouri S&T was supported by

the University of Missouri Research Boards and by the National Science Foundation Grant No.DMR-0704981.

SECTION

2. CONCLUSIONS

This thesis work presented the detailed theoretical and experimental investigations of the intentionally introduced disorder in a photo-sensitive multi-mode optical fiber. Starting with the microscopic model of photo-sensitivity in the germanium-doped silica fibers, we studied the statistical properties of the volume disorder and described an experimental procedure to manipulate it.

Transmission of light through a fiber is commonly described with coupled-power or coupled-mode theories. However, both theories by themselves failed in the case of fiber with the artificial correlated disorder considered in this work. To properly describe the novel fiber, hybrid coupled-power -coupled-mode theory was developed. It simultaneously accounts for such effects as birefringence and co- and cross-polarization mode coupling. It was shown that after $\sim 10cm$ distance, the power can be equally distributed over all co-propagating modes including both polarization channels.

The theory developed in this work has been corroborated in experiment, where it was also shown that a thorough mode mixing can be accomplished without significant radiative losses. This makes our fibers with custom-made disorder suitable for such applications as e.g. hardware encryption in data transmission and power-management in high-power fiber laser systems. The complete mode mixing is also required to achieve the maximum information capacity in Multi-Input Multi-Output (MIMO) transmission via the multi-mode optical fibers.

BIBLIOGRAPHY

[1] W. K. Johnston. The birth of fiberoptics from "light guiding". *J. of Endourology*, 18:425–426, 2004.

[2] A. G. Bell. Apparatus for signaling and communicating called "photophone". *US patent*, 235199, 1880.

[3] D. Colladon. Daniel colladon's light fountain of light pipe. *Comptes rendus Academie des sciences*, 14, 1842.

[4] A. G. Bell. Photo-phone. 2013. http://en.wikipedia.org/wiki/Photophone.

[5] K. C. Kao and G. A. Hockham. Dielectric-fibre surface waveguides for optical frequencies. *Proc. IEE*, 113:1151 – 1158, 1966.

[6] J. Hecht. *City of light the story of fiber optics*. Oxford University Press, 1999.

[7] H. Kogelnik. High-capacity optical communications: personal recollections. *IEEE Journal of Selected Topics in Quantum Electronics*, 6:1279 – 1286, 2000.

[8] R. J. Essiambre and R. W. Tkach. Capacity trends and limits of optical communication networks. *Proc. of IEEE*, 100:1035 – 1055, 2012.

[9] G. J. Foschini and M. J. Gans. On limits of wireless communications in a fading environment when using multiple antennas. *Wireless Personal Comm.*, 6:311–335, 1998.

[10] E. Telatar. Capacity of multi-antenna gaussian channels. *Euro. Trans. Telecomm.*, 10:585–595, 1999.

[11] H. R. Stuart. Dispersive multiplexing in multimode optical fiber. *Science*, 289:281–283, 2000.

[12] P. C. Becker, N. A. Olsson, and J. R. Simpson. *Erbium-doped fiber amplifiers, fundamentals and technology*. New York: Academic Press, 1990.

[13] J. Tang. The channel capacity of a multispan dwdm system employing dispersive nonlinear optical fibers and an ideal coherent optical receiver. *J. Lightwave Tech.*, 20:1095–1101, 2002.

[14] L. G. L. Wegener. The effect of propagation nonlinearities on the information capacity of wdm optical fiber systems: Cross-phase modulation and four-wave mixing. *Physica D*, 189:81–99, 2004.

[15] M. H. Taghavi, G. C.Papen, and P. H. Siegel. On the multiuser capacity of wdm in a nonlinear optical fiber: Coherent communication. *Information Theory*, 52:5008–5022, 2006.

[16] D. J. Richardson, J. M. Fini, and L. E. Nelson. Space-division multiplexing in optical fibres. *Nature Photonics*, 7:354–362, 2013.

[17] S. Iano, T. Sato, S. Sentsui, T. Kuroha, and Y. Nishimura. Multicore optical fiber. *Proc. Opt. Fiber Commun. Conf.*, pages 46–48, 1979.

[18] S. Berdague and P. Facq. Mode division multiplexing in optical fibers. *Appl. Opt.*, 21:1950–1955, 1982.

[19] X. Shen, J. M. Kahn, and M. A. Horowitz. Compensation for multimode fiber dispersion by adaptive optics. *Opt. Lett.*, 30:2985–2987, 2005.

[20] P. J. Winzer and G. J. Foschini. Mimo capacities and outage probabilities in spatially multiplexed optical transport systems. *Wireless Communication*, 6:2612 – 2621, 2011.

[21] S. H. Simon, A. L. Moustakas, M. Stoychev, and H. Safar. Communication in a disordered world. *Phys. Today*, 54:38–43, 2001.

[22] R. C. J. Hsu, A. Tarighat, A. Shah, A. H. Sayed, and B. Jalali. Capacity enhancement in coherent optical mimo (comimo) multimode fiber links. *IEEE Comm. Lett.*, 10:195–197, 2006.

[23] L. Raddatz, I. White, D. Cunningham, M. Nowell, M. Tan, and S. .Wang. Fiber-optic m-ary modulation scheme using multiple light sources. *Technical Digest*, 198-199, 1997.

[24] H. Blow, F. Buchali, and A. Klekamp. Electronic dispersion compensation. *J. Lightwave Tech.*, 26:158–167, 2008.

[25] H. Haunstein, W. Sauer-Greff, A. Dittrich, K. Sticht, and R. Urbansky. Principles for electronic equalization of polarization-mode dispersion. *J. Lightwave Tech.*, 22:1169–1182, 2004.

[26] L. Raddatz, D. White, R. V. pdenty, and D. G. Cunningham. High bandwidth data transmission in multimode fibre links using subcarrier multiplexing with vcsels. *Electronics Lett.*, 34:686–688, 1998.

[27] J. Kahn, K. P. Ho, and M. B. Shemirani. Mode coupling effects in multi-mode fibers. *Proceedings of Optical Fiber Communication Conference*, 2012.

[28] R. Olshansky. Mode coupling effects in graded-index optical fibers. *Appl. Opt.*, 14:935–945, 1975.

[29] D. Marcuse. Coupled power equations for lossy fibers. *Appl. Opt.*, 17:3232–3237, 1978.

[30] J. A. Jay. An overview of macrobending and microbending of optical fibers. 2010.

[31] J. W. Berthold. Historical review of microbend fiber-optic sensors. *JOURNAL OF LIGHTWAVE TECHNOLOGY*, 13:1193–1199, 1995.

[32] A. F. Garito, J. Wang, and R. Gao. Effects of random perturbations in plastic optical fibers. *Science*, 281:962–967, 1998.

[33] K. O. Hill and G. Meltz. Fiber bragg grating technology: Fundamentals and overview. *J. Lightwave Techn.*, 15:1263–1276, 1997.

[34] A. Kamal and P. St. J. Russell. Physical origins and general dielectric tensor of photoinduced anisotropy in optical fibers and bulk glasses. *J. Opt. Soc. Am. B*, 11:1576–1584, 1994.

[35] T. Erdogan. Fiber grating spectra. *J. Lightwave Techn.*, 15:1277–1294, 1997.

[36] D. Marcuse. Rayleigh scattering and the impluse response of optical fiber. *Bell Syst. Tech. J.*, 53:705–715, 1974.

[37] J. C. Dainty. *Topics in applied physics*. Springer, 1984.

[38] T. Erdogan and V. Mizrahi. Characterization of uv-induced birefringence in photosensitive ge-doped silica optical fibers. *J. Opt. Soc. Am. B*, 11:2100–2105, 1994.

[39] R. K. Luneburg. *Mathematical Theory of Optics*. Univ. California Press, 1964.

[40] D. Marcuse. *Theory of Dielectric Optical Waveguides*. Academic, 1974.

[41] H. Cao. Review on latest developments in random lasers with coherent feedback. *J. Phys. A: Math. Gen.*, 38:10497–10535, 2005.

[42] S. E. Skipetrov. Disorder is the new order. *Nature*, 432:285–286, 2004.

[43] A. Lagendijk, B. van Tiggelen, and D. S. Wiersma. Fifty years of anderson localization. *Phys. Today*, 62:24–29, 2009.

[44] J. A. Sanchez-Gil, V. D. Freilikher, A. A. maradudin, and I. Yurkevich. Reflection and transmision of waves in surface disordered waveguieds. *Phys. Rev.*, 59:5915–5925, 1999.

[45] E. I. Chaikina, S. Stepanov, and A. G. Navarrete. Formation of angular power profile via ballistic light transport in multi-mode optical fiber with corrugated surface. *Phys. Rev. B*, 71:085419, 2005.

[46] A. A. Chabanov, M. Stoytchev, and A. Z. Genack. Statistical signatures of photon localization. *Nature*, 404:850–853, 2000.

[47] J. Topolancik, B. Ilic, and F. Vollmer. Random high-q cavities in disordered photonic crystal waveguides. *Appl. Phys. Letters*, 91, 2007.

[48] O. Shapira and B. Fischer. Localization of light in a random-grating array in a single-mode fiber. *J. Opt. Soc. Am. B*, 22:2542–2552, 2005.

[49] C. Lu, J. Cui, and Y. Cui. Reflection spectra of fiber bragg gratings with random fluctuations. *Optical Fiber Technology*, 14:97–101, 2008.

[50] C. J. S. Matos, L. de S. Menezes, A. M. Brito-Silva, M. A. Martinez Gámez, A. S. L. Gomes, and C. B. de Araújo. Random laser action in the core of a photonic crystal fiber. *Opt. Phot. News*, 19:27–27, 2008.

[51] M. Gagné and R. Kashyap. Demonstration of a 3 mw threshold er-doped random fiber laser based on a unique fiber bragg grating. *Opt. Express*, 17:19067–19074, 2009.

[52] S. K. Turitsyn, S. A. Babin, A. E. El-Taher, P. Harper, D. V. Churkin, S. I. Kablukov, J. D. Ania-Cast nón, V. Karalekas, and E. V. Podivilov. Random distributed feedback fibre laser. *Nature Photonics*, 4:231–235, 2010.

[53] H. Cao, Y. Zhao, S. T. Ho, E. W. Seelig, Q. H. Wang, and R. P. H. Chang. Random laser action in semiconductor powder. *Phys. Rev. Lett.*, 82:2278–2281, 1999.

[54] N. Lizarraga, N. Puente, E. Chaikina, T. Leskova, and E. Mendez. Single-mode er-doped fiber random laser with distributed bragg grating feedback. *Opt. Express*, 17:395–404, 2009.

[55] J. W. Goodman. *Speckle Phenomena in Optics: Theory and Applications*. Coberts & Co, Englewood, 2007.

[56] P. W. Anderson. Absence of diffusion in certain random lattices. *Phys. Rev.*, 109:1492–1505, 1958.

[57] B. Crosignani, A. Saar, and A. Yariv. Coherent backscattering and localization in a single-mode fiber with random imperfections. *Phys. Rev. A*, 43:3168–3171, 1991.

[58] H. C. van de Hulst. *Light scattering by small particles*. Dover,New York, 1981.

[59] L. B. Jeunhommer. *Single-mode Fiber Optics*. Marcel Dekker. Inc, 1990.

[60] A. Ishimaru. *Wave Propagation and Scattering in Random Media*. Academic Press, 1978.

[61] H. Cao. Lasing in disordered media. In E. Wolf, editor, *Progress in optics*, volume 45. North Holland, 2003.

[62] I. M. Vellekoop, A. Lagendijk, and A. P. Mosk. Exploiting disorder for perfect focusing. *Nat. Phot.*, 4:320–322, 2010.

[63] M. Limonov and R. De La Rue, editors. *Optical properties of photonic structures: interplay of order and disorder*. Francis & Taylor, 2012.

[64] M. Fink. Time reversed acoustics. *Phys. Today*, 50:34–40, 1997.

[65] A. Amphawan. Holographic mode-selective launch for bandwidth enhancement in multimode fiber. *Opt. Express*, 19:9056–9065, 2011.

[66] M. Nazarathy and A. Agmon. Coherent transmission direct detection mimo over short-range optical interconnects and passive optical networks. *J. Lightwave Techn.*, 26:2037–2045, 2008.

[67] M. Greenberg, M. Nazarathy, and M. Orenstein. Multimode fiber as random code generator – application to massively parallel mimo transmission. *J. Lightwave Techn.*, 26:882–890, 2008.

[68] N. P. Puente, E. I. Chaikina, S. Herath, and A. Yamilov. Fabrication, characterization and theoretical analysis of controlled disorder in the core of the optical fibers. *Applied Optics*, 50:802–810, 2011.

[69] D. Gloge. Optical power flow in multimode fibers. *Bell Syst. Tech. J.*, 51:1767–1783, 1972.

[70] A. M. Vengsarkar, Q. Zhong, D. Inniss, W. A. Reed, P. J. Lemaire, and S. G. Kosinski. Birefringence reduction in side-written photoinduced fiber devices by a dual-exposure method. *Opt. Lett.*, 19:1260–1262, 1994.

[71] N. Belhadj, Y. Park, S. LaRochelle, K. Dossou, and J. Aza na. Uv-induced modification of stress distribution in optical fibers and its contribution to bragg grating birefringence. *Opt. Express*, 16:8727–8741, 2008.

[72] G. J. Foschini and C. D. Poole. Statistical theory of polarization dispersion in single mode fibers. *J. Lightwave Tech.*, 9:1439–1456, 1991.

[73] J. P. Gordon and H. Kogelnik. Pmd fundamentals: Polarization mode dispersion in optical fibers. *Proc. Nat. Acad. Sc.*, 97:4541–4550, 2000.

[74] L. Mandel and E. Wolf. *Optical coherence and quantum optics*. Cambridge University Press, 1995.

[75] O. Korotkova. Changes in statistics of the instantaneous stokes parameters of a quasi-monochromatic electromagnetic beam on propagation. *Opt. Comm.*, 261:218–224, 2006.

[76] H. Cao. Lasing in random media. 2003.

[77] A. E. Ennons. Speckle interferomentry. 1984.

VITA

Sumudu Herath was born in Kurunegala, Sri Lanka and completed her high school education in Visakha Vidyalaya, Colombo. She received her Bachelor's Degree in Physics and Statistics from the University of Peradeniya, Sri Lanka in March 2007. She was a member of both the track and field athletic team and the hockey team at both institutions. She was awarded as the best athlete several times and the teams she played on gained national recognition. She was a school prefect and served as a member of the Physical society and several clubs.

After she moved to the United States, Sumudu enrolled as a graduate student at Missouri University of Science and Technology, Rolla in 2009. In May 2013, she received her Master of Science Degree in Physics. Upon completion of this degree, she pursued a Ph.D. on disordered fiber with her research adviser, Dr.Alexey Yamilov. While there, she worked as a research assistant to Dr. Yamilov and presented her research at several scientific meetings. During her graduate studies, Sumudu Herath has coauthored several publications.

She served as a teaching assistant for the Physics Department at Missouri S& T and received an Outstanding Graduate Teaching Assistant award for the 2012 academic year. She was presented her Ph.D. degree in December 2013.